Molecular Plant
Research article

CellPress
Partner Journal

Hormonal regulation of cell fate plasticity of xylem-pole-pericycle lineage in *Arabidopsis* roots

Xin Wang[1,3,4,*], Lingling Ye[1,4], Jing Zhang[1,5], Charles W. Melnyk[2] and Ari Pekka Mähönen[1,*]

[1]Organismal and Evolutionary Biology Research Programme, Faculty of Biological and Environmental Sciences and Viikki Plant Science Centre, University of Helsinki, Helsinki, Finland

[2]Department of Plant Biology, Linnean Center for Plant Biology, Swedish University of Agricultural Sciences, Uppsala, Sweden

[3]Present address: Faculty of Synthetic Biology, Shenzhen University of Advanced Technology, Shenzhen 518107, China

[4]Present address: Institute of Emerging Agricultural Technology, Shenzhen University of Advanced Technology, Shenzhen 518107, China

[5]Present address: Department of Plant Biology and Ecology, College of Life Sciences, Nankai University, Tianjin 300071, China

***Correspondence: Xin Wang (wangxin@suat-sz.edu.cn), Ari Pekka Mähönen (aripekka.mahonen@helsinki.fi)**

https://doi.org/10.1016/j.molp.2025.09.006

ABSTRACT

In *Arabidopsis* roots, xylem-pole-pericycle (XPP) cells exhibit dual cell fates by contributing to both lateral root (LR) and cambium formation. Despite the significant progress in understanding these processes individually, the mechanism deciding between these two fates and its contribution on root architecture and secondary growth remain unknown. In this study, we combined lineage tracing with molecular genetics to study the regulation of fate plasticity of XPP cell lineage. We showed that developmentally arrested lateral root primordium (LRP) that fails to emerge as a lateral root gradually obtains cambium identity, thus contributing to secondary growth. Conversely, procambium identity within XPP cells can be reverted to LR identity when simulated by auxin, a key player in LR development. This competence for auxin-induced LR formation from XPP cells, termed LR potency, however, decreases as the root matures. We found that key cambium regulators play critical roles in shaping LR potency not only by promoting cambium identity and activation but also by inhibiting LR formation. Consistently, corresponding mutants with impaired cambium activity display broader LR potency. Moreover, cytokinins, essential players in cambium development, facilitate the identity transition of LRP to cambium and reduce LR potency through key cambium regulators. Taken together, these findings highlight the inherent fate plasticity of XPP cell lineage and elucidate how plant hormones influence root architecture and secondary growth through balancing the two cell fates of XPP cells.

Key words: xylem-pole-pericycle cells, lateral root, cambium, cell fate, plasticity, lineage tracing, auxin, cytokinins

Wang X., Ye L., Zhang J., Melnyk C.W., and Mähönen A.P. (2025). Hormonal regulation of cell fate plasticity of xylem-pole-pericycle lineage in *Arabidopsis* roots. Mol. Plant. **18**, 1759–1776.

INTRODUCTION

In *Arabidopsis* roots, the xylem-pole-pericycle (XPP) cells are regarded as an extended meristem (Beeckman et al., 2001; Himanen et al., 2004; Parizot et al., 2008). In tissue culture conditions, whole seedlings can be regenerated from XPP cells (Atta et al., 2009; Sugimoto et al., 2010). Under the normal conditions, XPP cells exhibit two distinct cell fates. Within the root tip of *Arabidopsis*, a cluster of XPP cells are designated as a prebranch site. This site is primed for the subsequent formation of a lateral root primordium (LRP) (De Smet et al., 2007; Moreno-Risueno et al., 2010; Van Norman et al., 2013; Xuan et al., 2020), which contributes to root architecture upon breaking overlying tissues and emerging as a lateral root (LR). XPP cells not participating in LRP formation gradually adopt the identity of cambium (referred to as cambium-fate XPP cells), contributing to secondary growth (Smetana et al., 2019). Lineage tracing studies have shown that XPP cells from their circumferential positions give rise to both vascular cambium, which generates vascular tissues, and cork cambium, which produces the protective periderm layer (Smetana et al., 2019).

The key plant hormones, auxin and cytokinin, play antagonistic roles in LR development. Auxin signaling influences every stage of LR development, including prebranch site formation, founder cell specification, LR initiation, as well as the subsequent patterned cell divisions of LRP, culminating in the emergence of LR by

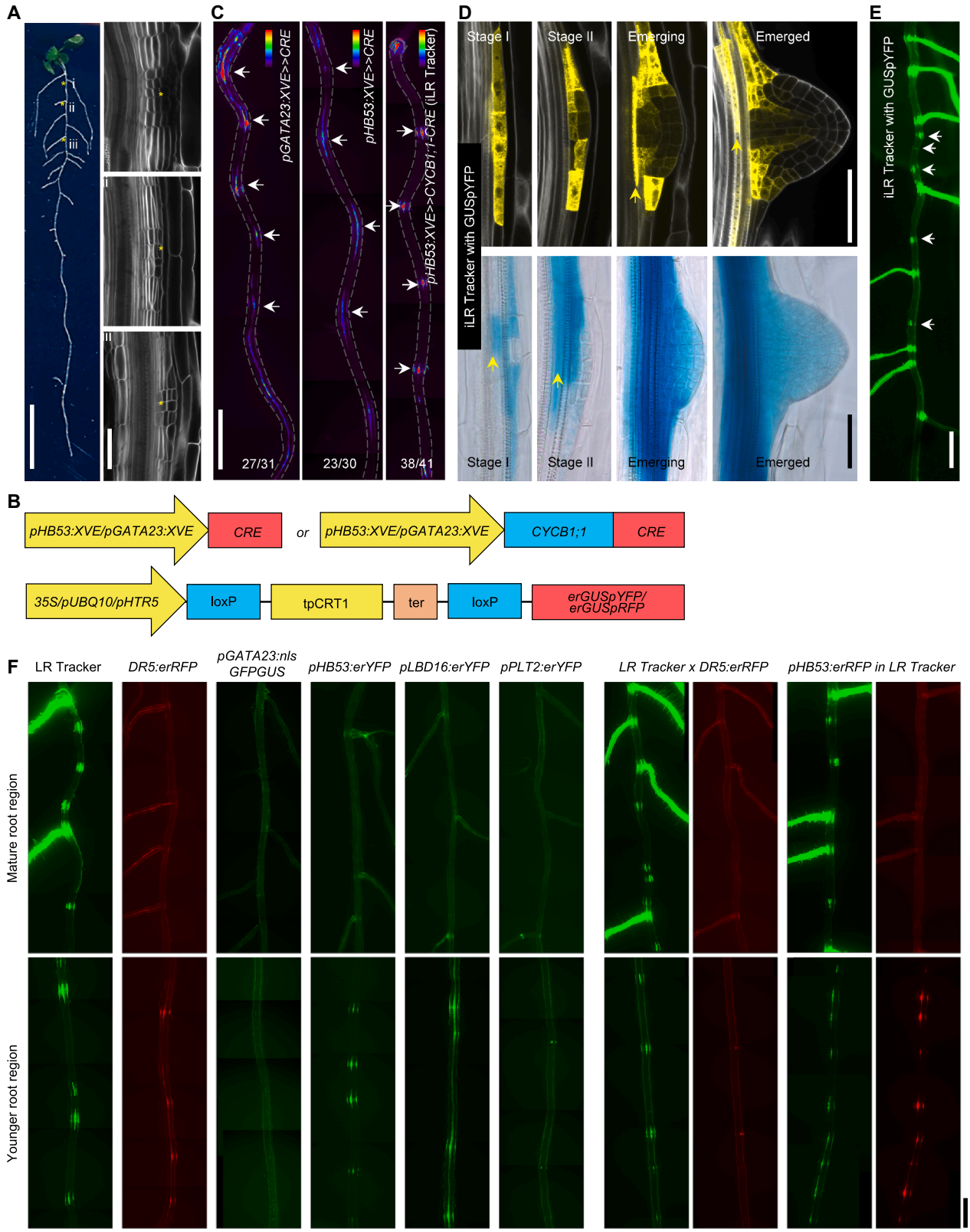

Figure 1. Establishment of CRE-loxP-based LR-tracing systems

(A) Left, an overview of root architecture of an 8-day-old seedling with arrested LRPs. Right, a close-up view of developmentally arrested LRPs imaged by confocal microscopy. Yellow asterisks indicate relative positions of arrested LRPs in the root.

(legend continued on next page)

penetrating through overlying tissues (Du and Scheres, 2018; Jing and Strader, 2019; Motte et al., 2019). Auxin treatment can induce *de novo* LR formation from XPP cells in a manner independent of the prebranching mechanism (Dubrovsky et al., 2008; Moreno-Risueno et al., 2010). Conversely, cytokinins impede LRP initiation, disrupt proper positioning along the primary root, and impair subsequent development (Li et al., 2006; Laplaze et al., 2007; Marhavý et al., 2011; Bielach et al., 2012; Chang et al., 2013, 2015; Jing and Strader, 2019). While cytokinins exhibit inhibitory effects on LR development, they promote the cambium activation and serve as rate-limiting regulators of cambial activity and secondary growth (Matsumoto-Kitano et al., 2008; Ye et al., 2021). Cytokinin treatment can prematurely activate cambium for secondary growth (Ye et al., 2021). Therefore, while auxin promotes XPP cells to develop into LRs, cytokinins favor cambium formation.

It has been shown that a significant portion of slowly developing LRPs fail to progress into emergence and instead enter a silent state (Dubrovsky et al., 2006). For these developmentally arrested LRPs, their ultimate fate is uncertain. In addition, how internal and external stimuli, such as auxin and cytokinin, modulate the ratio of arrested LRPs to the number of emerged LRs is also unknown. Although auxin treatment can induce *de novo* LR formation from XPP cells (Dubrovsky et al., 2008, 2011), this auxin-induced LR formation potential, termed LR potency here, decreases as root matures by an unknown mechanism. Therefore, to fully understand cell fate plasticity of the XPP lineage and its influence on root architecture and secondary growth, these two developmental processes need to be investigated in an integrated manner.

The CRE-loxP site-specific recombination system, in which CRE recombinase recognizes a 34-bp DNA sequence known as loxP and mediates recombination between two loxP sites, has been widely used for lineage tracing by conditionally activating a reporter gene in a target cell, thereby enabling genetic labeling of all its progeny (Kretzschmar and Watt, 2012). In this study, assisted by the novel CRE-loxP-based lineage tracing systems which specifically and permanently label an LRP, we revealed the interchangeable nature of these two XPP cell fates and its regulation. The developmentally arrested LRPs eventually relinquish their original identity and adopt cambium identity. Conversely, the procambium identity within XPP cells can be reverted into LR identity by auxin application. As the root matures, the LR potency decreases, due to the inhibitory effect of gradually accumulating cambium regulators. Cytokinins, consistent with their key roles in cambium development, promote the arrest of young LRPs and facilitate the transition from LRP identity to cambium identity. Cytokinins also lower LR potency via inducing key cambium regulators. These findings not only underscore the notable cell fate plasticity of the XPP lineage but also revealed how auxin and cytokinins balance these two cell fates between LR and cambium, thereby influencing root architecture and secondary growth.

RESULTS

Developing CRE-lox based LR-tracing systems

Currently, there is no system available that allows for LR-specific, permanent labeling to facilitate the tracking of the cell fate plasticity of developing LRP. Arrested LRPs, in particular, are challenging to detect and track, especially in the more mature part of the root (Figure 1A). To overcome this, we developed an inducible CRE-loxP-based LR-tracing system. LR-specific inducible promoters were used to drive CRE recombinase expression, inducing DNA sequence recombination between two loxP sites and thereby activating transcription of a reporter gene under a constitutive promoter, which allows the labeling of cells and their progeny in the LRP lineage (Figure 1B). We first assessed two LR-specific promoters, *pGATA23* (De Rybel et al., 2010) and *pHB53* (González-Grandío et al., 2017; Serrano-Ron et al., 2021), and made estradiol inducible versions of them, *pGATA23:XVE* and *pHB53:XVE*. We fused each inducible promoter with the CRE recombinase coding sequence and introduced the constructs into a prescreened *35S:loxP-erGUSpYFP* background (Figure 1B). The erGUSpYFP fusion contain endoplasmic reticulum (ER)-localized GUSplus reporter fused with YFP reporter thus allowing flexible analysis of the clones. As both promoters exhibit activities in the stage I LRP, it is therefore possible the whole LRP/LR can be marked after CRE-mediated recombination and reporter gene activation. In T1 transgenic plants, we observed that after a 1-day estradiol treatment, YFP-labeled LR/LRP clones were efficiently induced on the convex side of

(B) A schematic of LR-tracing systems. CRE recombinase variants are induced with two different inducible, LR-specific promoters. CRE catalyzes recombination between two loxP sites leading to constitutive expression of reporters driven by *35S*, *pUBQ10*, or *pHTR5*.
(C) A comparison of distinct LR-specific inducible promoters and CRE recombinase variants. Three-day-old T1 seedlings grown on standard half-strength growth medium (½GM) were transferred to induction medium for 1 day before stereo microscopy. Numbers represent the frequency of the observed types of YFP clones in independent T1 samples. Roots are outlined with gray dashed lines. Combination of *pHB53:XVE>>CYCB1;1-CRE* and *35S:loxP-erGUSpYFP*, named iLR Tracker, was used in the subsequent experiments. We named the combination of *pHB53:CYCB1;1-CRE* and *35S:loxP-erGUSpYFP* as LR Tracker (Supplemental Figure 1). White arrows mark each YFP clone associated with an LRP.
(D) In the iLR Tracker, a detailed confocal inspection and GUS staining revealed that LRs/LRPs are faithfully marked at various stages. Three-day-old seedlings grown on ½GM were induced for 1 day, followed by analysis using confocal microscopy or GUS staining. GUS staining revealed a total of 467 LRs/LRPs, of which 406 showed clear GUS signals. All 406 GUS-marked clones accurately labeled LRs/LRPs (n = 42). Yellow arrows indicate unspecific clones associated with overlying LRs/LRPs.
(E) An example showing arrested LRPs (white arrows) in the upper region of a 10-day-old root, as visualized by the iLR Tracker under a fluorescence stereo microscope. Three-day-old seedlings grown on ½GM were first given 1 day induction then transferred to estradiol-free medium for another 6 days.
(F) Comparison of LR Tracker with other LR-related reporters. Seedlings were grown on ½GM for 10 days before imaging both the younger root region (below the first emerged LRP) and the mature root region (below the hypocotyl) using fluorescence stereo microscopy. For direct comparison, the LR Tracker line was crossed with *DR5:erRFP* and analyzed in the F1 generation. The *pHB53:erRFP* construct was introduced into the LR Tracker background, and T1 transgenic seedlings were analyzed. For each comparison, 10–15 seedlings were examined.
Scale bars, 1 cm (**A**, left), 1 mm **(C**, **E**, and **F)**, 50 μm (**A**, right; **D)**.

the root curve. Comparative analysis revealed that, in contrast to *pHB53*, the *GATA23* inducible promoter induced continuous YFP signals in the younger part of the root, resembling its native promoter's expression pattern (De Rybel et al., 2010; Vermeer et al., 2014). Consequently, *pHB53:XVE* exhibited more specific labeling of LRs/LRPs compared to *pGATA23:XVE* (Figure 1C).

Despite being more specific for LRs/LRPs, YFP clones generated by *pHB53:XVE* marked a relatively broad domain beyond the LR/LRP itself (Figure 1C). We then tested the CYCB1;1-CRE construct (Smetana et al., 2019) to restrict the recombinase activity specifically to mitotic cells at the G2/M phase of the cell cycle (Figure 1B) (Colón-Carmona et al., 1999; Marrocco et al., 2009; Smetana et al., 2019). Compared with CRE, the CYCB1;1-CRE enabled the generation of smaller yet LR/LRP-specific clones (Figure 1C). Therefore, the CYCB1;1-CRE recombinase was used for all further studies. Detailed confocal examination revealed nearly 100% (359/360 clones in 38 roots) of YFP clones specifically marked LRs/LRPs, with over 80% (250/298 clones in 36 roots) of analyzed LRs/LRPs exhibiting YFP signal (Figure 1D). GUS reporter assay showed a similar result (Figure 1D). With such an inducible LR-tracing system, the arrested LRP can be easily detected and tracked just under a fluorescence stereo microscope (Figure 1E). We named this inducible LR-tracing system as iLR Tracker.

In addition, by utilizing the HB53 native promoter, we also established a stable LR-tracing system (named LR Tracker) and validated its reliability in LR/LRP tracing (Supplemental Figure 1). To demonstrate versatility of this system, we grew the LR Tracker line under different nutritional, hormonal, or stress conditions (Supplemental Figure 2). In addition to expected root architecture phenotypes (Zhang et al., 1999; Duan et al., 2013; Kim et al., 2022), the LRs/LRPs under each condition were clearly labeled with YFP, indicating the wide compatibility of this system with various growth conditions (Supplemental Figure 2). With the LR Tracker, the root architecture can be easily visualized and quantified under a fluorescence stereo microscope, significantly simplifying LR-related quantification compared to conventional methods. For example, quantifying the LR/LRP number within a fixed region of a 7-day-old root took about 25s with the LR Tracker, while for the same region of the same root, standard microscopy required more than 5 min, without including time spent for sample preparation (Supplemental Figure 3A). Implementation of such a system also improves the accuracy of LR/LRP quantification: an average of 30 LRs/LPRs could be detected using the LR Tracker under a fluorescence stereo microscope, compared with 25 LRs/LRPs with standard microscopy (Supplemental Figure 3B). This is likely due to the tendency of LRPs to be overlooked in the latter case.

Occasionally, we observed unspecific induction of YFP/GUS in the vascular cells underneath an LR/LRP in both systems (Figure 1D and Supplemental Figure 1). However, this did not affect LR/LRP identification or quantification as these non-specific expressions were consistently associated with the overlaying YFP/GUS-marked LR/LRP. We also noticed that LRs/LRPs were not always fully marked by YFP/GUS expression (Figure 1D and Supplemental Figure 1). This might be due to either loss of recombination events in some LRP cells, likely caused by the cell-cycle-dependent regulation of CYCB1;1-CRE stability, or by the expression preference of the 35S promoter, which drives the YFP/GUS expression after the recombination. Additionally, the youngest LRPs near the root tip exhibited weak signal, likely because these LRPs might not have enough time to accumulate a sufficient amount of YFP/GUS for visualization after recent recombination events (Supplemental Figure 1). Thus, we typically quantified LRs/LRPs within a fixed region of the root rather than the entire root. In the T2 generation of the LR Tracker lines, we also noticed a small portion of seedlings (ranging from 0.3%–2.8% for different lines) showing YFP expression in the whole seedling, indicating unspecific recombination events in the germ cell line. In conclusion, iLR Tracker and LR Tracker facilitate convenient and high throughput, real-time LR development observation and quantification in an intact root, just under a fluorescence stereo microscope.

Comparison between the LR Tracker and conventional LR reporters

We then compared the LR Tracker line with the known LR reporters, including *DR5:erRFP*, *pGATA23:nlsGFPGUS*, *pLBD16:erYFP*, *pPLT2:erYFP*, and *pHB53:erYFP* (Figure 1F). In the younger root regions where LRP initiation and development occur, *DR5*, *pGATA23*, and *pLBD16* exhibit broad transcriptional activity that extends beyond the LRP itself. In contrast, *pHB53* shows LRP-specific expression, while *pPLT2* is restricted to the later stages of LRP development (Figure 1F, lower panel). However, none of these reporters show expressions in the arrested LRPs in the mature root region during secondary growth, as the LR Tracker does (Figure 1F, upper panel). These results were further validated by a direct comparison with the generated double reporter lines of *LR Tracker* x *DR5:erRFP* and the *pHB53:erRFP;LR Tracker*. In the mature root region, the same arrested LRPs show YFP signals but no RFP signals (Figure 1F, upper right panel). Therefore, the LR Tracker enables the specific and permanent labeling of LRs/LRPs, which makes it a powerful tool for root architecture studies, especially when arrested LRPs are of interest. Our results also indicate that arrested LRPs will finally lose their LRP identity.

Arrested LRPs eventually acquire cambium identity

Taking advantage of the iLR Tracker, we were able to reliably monitor the development of individual LRP over extended time periods. We first gave a 1-day estradiol treatment to 3-day-old seedlings to induce YFP expression in LRP then transferred the seedlings to estradiol-free medium and tracked each YFP-marked LRP (in the upper root region of about 1 cm) over the following days, by using a fluorescence stereo microscope (Figure 2A–2C). In our growth conditions, LR emergence predominantly occurred between day 4 and day 7 in this root region (Figure 2C). At day 7, approximately half of all LRPs failed to grow out (Figure 2C). Intriguingly, the YFP sectors originating from these developmentally arrested LRPs gradually expanded radially along with the overall secondary growth (Figure 2D). Further examination post-GUS staining revealed a morphological shift of these LRP cells from cubic to thin-shaped cells due to periclinal cell divisions. Thus, the morphology and division pattern resemble cambial cells, although the cells are shorter than in cambium due to their origin from the short LRP cells (Figure 2E). Additionally, within the same observation

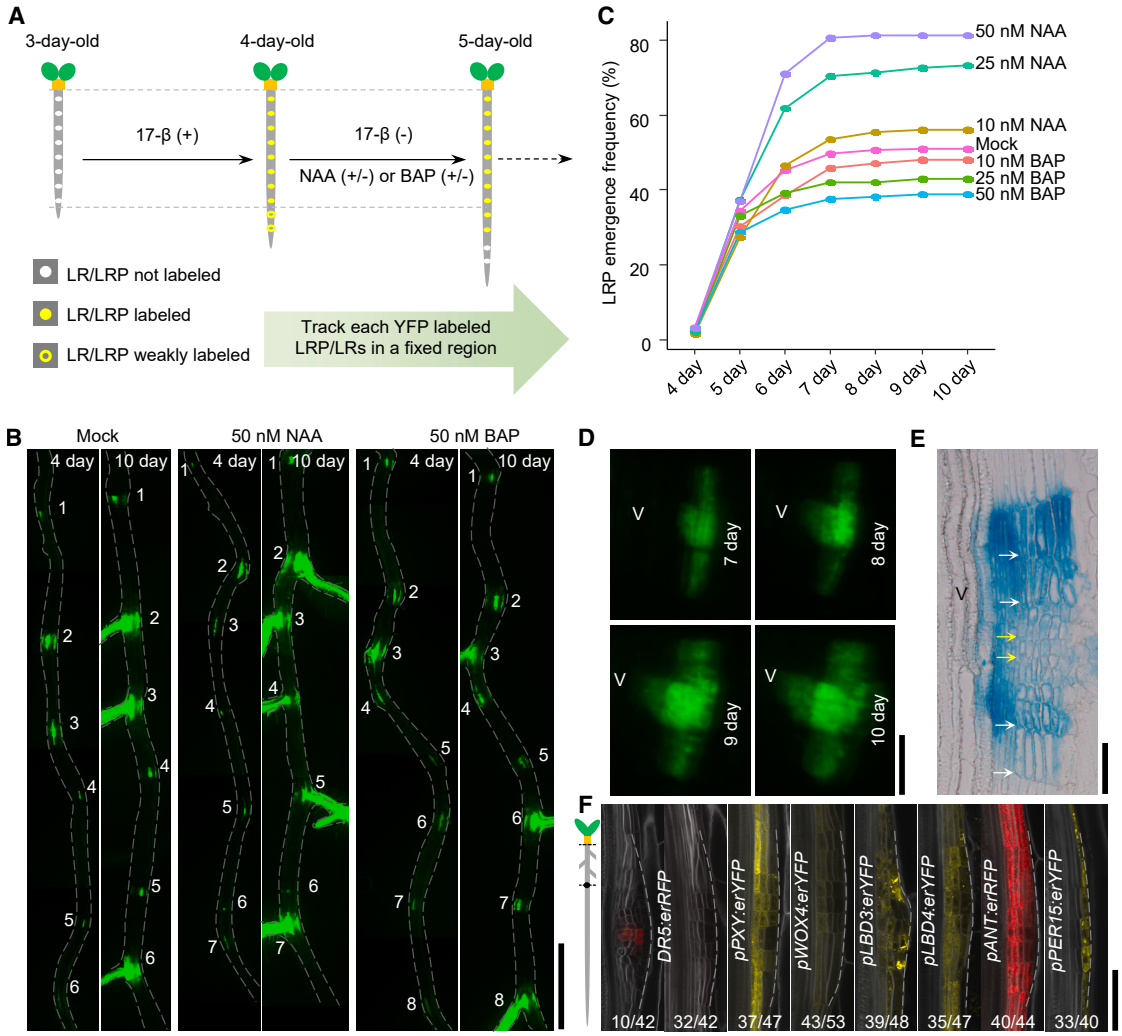

Figure 2. Arrested LRPs gradually acquire cambium identity

(A) A schematic showing the strategy used for LR/LPR tracing with the iLR Tracker. Three-day-old seedlings grown on ½GM were first induced for 1 day before transferring them to estradiol-free medium with/without phytohormones. After transferring, each LR/LRP was tracked under a fluorescence stereo microscope until the roots were 10 days old. Note, after a 1-day induction, the LRPs in the newly formed root region showing initially weak fluorescence (marked by yellow ring) were not followed. Therefore, a fixed root region marked between dashed lines was traced.

(B) Examples showing LR/LRP tracing in each root (outlined with gray dashed lines) under various conditions. In each panel, the same number labels the same LR/LRP when the root was 4 days old (left) and 10 days old (right).

(C) Quantifications of LRP emergence frequency over time in the presence of different concentrations of auxin (NAA) or cytokinin (BAP). In 4-day-old seedlings, auxin promotes and cytokinins inhibit LRP outgrowth in a dose-dependent manner. The data are shown as mean values calculated from a total LRP number of 146–313, based on 22 to 44 individual roots.

(D and **E)** Lateral view of an arrested LRP showing radially expanded YFP sector over time **(D)** and GUS sector in a 2-week-old root **(E)**. Note the shorter cells (yellow arrows) in the region that used to be an LRP compared to the longer cells (white arrows) in regions below and above **(E)**. V marks the vasculature region.

(F) While cambium markers showed their expression in arrested LRPs (outlined with gray dashed lines), DR5 expression was low, in the mature region of 7-day-old roots. The left schematic shows the region of the root where imaging was carried out. When the roots were 3 days old, their root tips were labeled, and 4 days later, only the root region above this label were sampled for confocal observation, without considering the maturing LRs. Numbers refer to the frequency of observed phenotypes.

Scale bars, 50 μm **(B**, **E**, and **F)** and 100 μm **(D)**.

region, the auxin responsive reporter DR5 exhibited low expression in most LRPs, suggesting reduced competence for continuing LR development (Figure 2F).

Lineage tracing and histological analysis suggest the arrested LRPs gradually acquire cambium-like properties to participate in the overall secondary growth. To validate this, we examined the expression of key vascular cambium regulator genes in LRPs, including the receptor kinase *PHLOEM INTERCALATED WITH XYLEM/TRACHEARY ELEMENT DIFFERENTIATION INHIBITORY FACTOR RECEPTOR* (*PXY/TDR*) (Fisher and Turner, 2007; Hirakawa et al., 2008), transcription factors

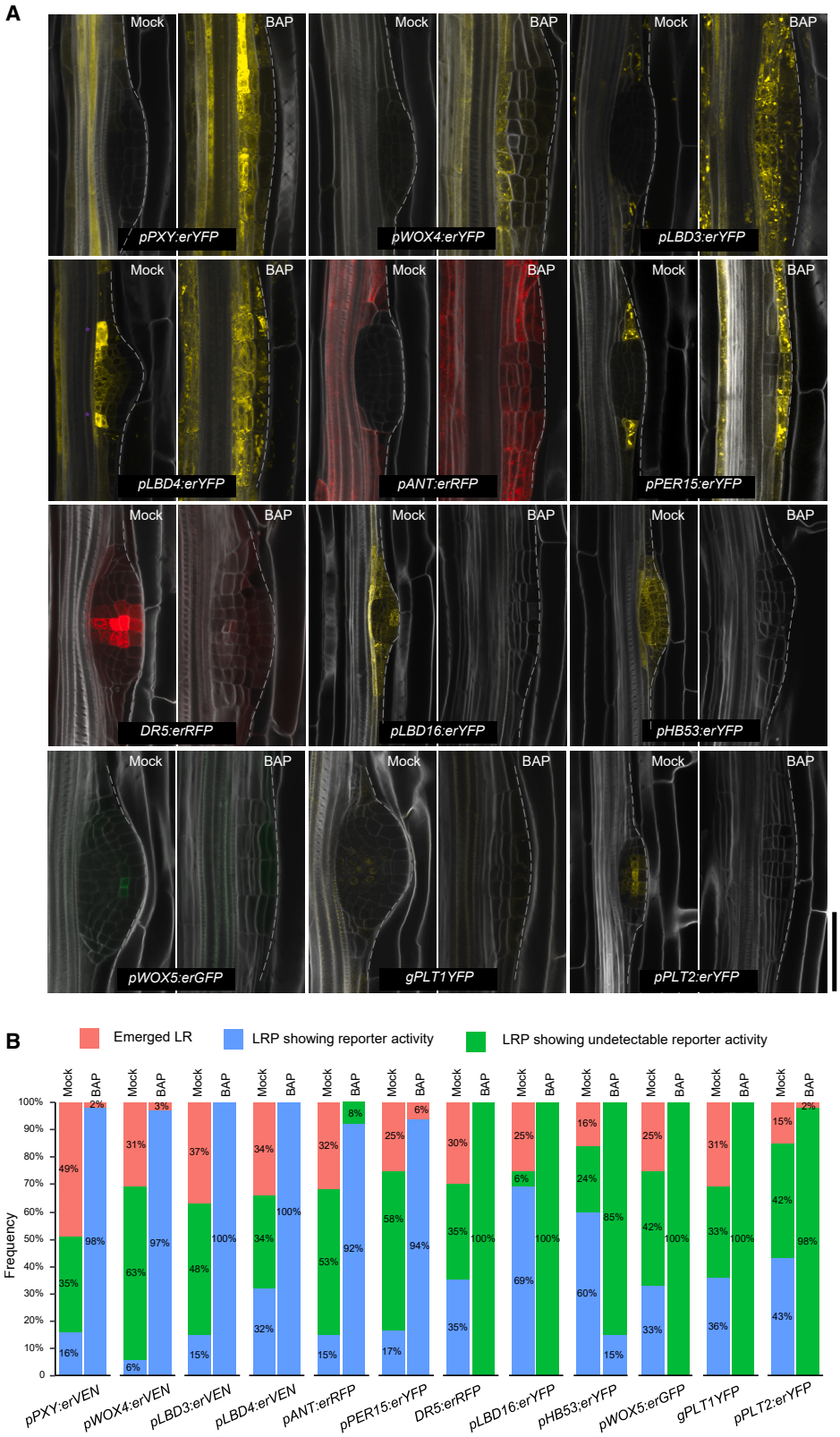

Figure 3. Cytokinins promote LRP to cambium identity transition

(A) Existing LRPs (outlined with gray dashed lines) acquired cambium identity with dampened expression of LR and root meristem reporters, after a 2-day 1-μM BAP treatment in 3-day-old seedlings. The LRPs from the newly grown part of the root after a 2-day growth were not included. Scale bar, 50 μm.
(B) Statistics of distinct reporter expression in LRPs with/without BAP treatment.

(legend continued on next page)

WUSCHEL RELATED HOMEOBOX 4 (*WOX4*) (Hirakawa et al., 2010), *LATERAL ORGAN BOUNDARIES DOMAIN 3* (*LBD3*), and *LBD4* (Ye et al., 2021), as well as *AINTEGUMENTA* (*ANT*) (Randall et al., 2015; Mäkilä et al., 2023; Eswaran et al., 2024). Additionally, we also included a cork cambium reporter driven by *PEROXIDASE15* (*PER15*) promoter (Xiao et al., 2020). While expression of most of these reporters were absent in the developing LRPs (see below, Figure 3), in the upper region of 7-day-old roots, most LRPs had obtained the expression of these vascular cambium reporters in the basal part of the primordia, adjacent to the protoxylem, as well as the *PER15* expression in the outmost layer, indicating a transition from LRP identity to cambial identity (Figure 2F).

Next, we studied the mechanisms by which an LRP gets arrested and obtain cambium identity. Given the importance of auxin in LR development (Benková et al., 2003; Bielach et al., 2012), we first performed time-course observation of auxin signaling changes in LRPs with the 3-day-old *DR5:erRFP* reporter line. While the normally developing LRPs quickly emerged as LRs within the following 3 days, about half of LRPs gradually lost the RFP signal (Supplemental Figure 4A). We therefore proposed that the failure to maintain an adequate auxin maximum in some LRPs may result in an arrest. Supporting this, transient inhibition of auxin signaling or its downstream targets involved in LR development promotes LRP arrest. This was achieved by conditionally expressing AXR3-1, a stable auxin signaling repressor (Rouse et al., 1998; Smetana et al., 2019), or LBD16-SRDX, a dominant-negative repressor of LBD16-mediated signaling (Goh et al., 2012), under the *pHB53:XVE* promoter. Transient inhibition of auxin transport using the auxin transport inhibitor 1-naphthylphthalamic acid (NPA) similarly promotes LRP arrest. After recovery, these arrested LRPs ultimately acquire cambium identity (Supplemental Figure 4B–4F). Moreover, our lineage tracing studies with the iLR Tracker line indicated that external auxin (naphthaleneacetic acid, NAA) supplementation to 4-day-old roots accelerated LRP outgrowth and reduced the number of arrested LRPs (Figure 2A–2C). Moreover, despite slowly acquiring cambial identity, a considerable portion (up to 20% depending on auxin levels) of arrested LRPs from 7-day-old roots could still be reactivated by additional auxin supplementation. The auxin signaling maximum in arrested LRPs could be rapidly reestablished within 12 h following 5 μM NAA application, leading to LR emergence within 3 days. In contrast, arrested LRPs in the control remained silent (Supplemental Figure 5). These results emphasize the cell fate plasticity of LRPs in response to internal and external stimuli (Supplemental Figure 5).

Arrested LRPs appeared to show increased resistance to auxin-triggered reactivation as the root matures. For example, relatively low levels of auxin (50 nM NAA) could efficiently reduce arrested LRP numbers when applied to a 4-day-old root (Figure 2B and 2C), but only reactivated a few of the arrested LRPs of a 7-day-old root. In the latter case, higher levels of auxin (up to 5 μM) were required for reactivation (Supplemental Figure 5A).

Cytokinins promote LRP to cambium identity transition

Cytokinins are known to inhibit LR initiation and development (Li et al., 2006; Laplaze et al., 2007; Marhavý et al., 2011; Bielach et al., 2012; Chang et al., 2013, 2015; Jing and Strader, 2019). Utilizing the iLR Tracker, we demonstrated that cytokinin treatment induces arrest of existing LRPs in a dose-dependent manner (Figure 2A–2C). Since cytokinins also promote cambial activation and secondary growth (Matsumoto-Kitano et al., 2008; Ye et al., 2021), we investigated whether cytokinin treatment facilitates the transition of LRP to cambium. Following a 2-day BAP treatment in 3-day-old seedlings, we observed morphological changes of LRP from a domed to flattened shape, accompanied with the emergence of expression of cambium reporters, including both vascular and cork cambium reporters, which were inactive in most LRP in the mock-treated roots (Figure 3). Unlike the other reporters, *LBD4* exhibited a heterogeneous expression across LRP in the absence of cytokinin, with stronger expression in the boundary domain. However, following benzylaminopurine (BAP) treatment, this expression pattern shifted to a uniform expression in the basal domain of LRP. Similarly, we observed a shift of *PER15* expression from the LRP boundaries to the out layers, after BAP treatment. Concurrently, LR and root meristem reporters tended to lose their expressions in LRP (Figure 3). Thus, cytokinin promotes LRP arrest and facilitates the acquisition of cambium identity. We also noticed that cytokinin-mediated acquisition of cambium identity in the LRP was accompanied by the cambial cell divisions and expanded expression of cambium regulators in the neighboring XPP cells (Supplemental Figure 6A), consistent with their central role as promoters of cambium activity (Matsumoto-Kitano et al., 2008; Ye et al., 2021).

In the 5-day-old roots with mock treatment, we found that a small subset of LRPs (less than 17%) showed expression of cambium regulators (except LRP-expressing *LBD4*), while approximately twice as many LRPs (about 35%) showed reduced DR5 reporter activity. These findings suggest that arrested LRPs begin to acquire cambium identity following a decline in auxin signaling (Figure 3B and Supplemental Figure 6B). Developmental arrest of LRP appears to take place during early stages, as suggested by their morphology (Supplemental Figure 6B). LRPs in the 3-day-old roots seem to be highly sensitive to cytokinin treatment, as indicated by efficient cytokinin-mediated LRP to cambium identity transition (Figure 3). Similarly, a previous report has shown that younger LRPs exhibit greater sensitivity to cytokinin compared to developmentally more advanced LRPs (Bielach et al., 2012). It is possible that in younger LRPs, the auxin maximum has not been stabilized, making them more susceptible to external interference. We also found that a 10-h BAP treatment was insufficient to trigger *PXY*/*TDR*, *WOX4*, and *ANT* expression in the most LRPs of 3-day-old seedlings, except for *LBD3*, which is a direct target of cytokinin signaling

Note that *LBD4* was expressed in the subdomain of LRPs (classified into the category "LRP showing undetectable reporter activity") in the mock treatment and throughout LPRs after BAP treatment **(A)**. The boundary expression of *LBD3* and *PER15* in some LRPs with the mock treatment **(A)** were classified into the category "LRP showing undetectable reporter activity." The frequency is calculated from a total LR/LRP number of 33–83, based on 8 to 16 individual roots.

(Ye et al., 2021) (Supplemental Figure 6C). For *PXY/TDR*, for example, a 24-h treatment was required to induce its expression in LRPs (Supplemental Figure 6D). In contrast, a time-course observation revealed that cytokinins were able to rapidly dampening auxin signaling in the LRPs of 3-day-old roots within 6 h (Supplemental Figure 6E). It has been shown that cytokinins are able to rapidly (about 1.5 h) deplete the auxin efflux carrier PINFORMED 1 (PIN1) from the plasma membranes through modulating PIN1 endocytic recycling and thus redirect auxin flow and inhibit LR organogenesis (Laplaze et al., 2007; Marhavý et al., 2011). It is thus likely that cytokinins promote the loss of LRP identity and the acquisition of cambium identity in a sequential manner.

We also investigated the cell fate transition of secondary LRPs (arising from mature LRs) in response to auxin and cytokinin using the iLR Tracker line. Ten-day-old seedlings grown on standard medium were transferred to induction medium for 1 day to initiate YFP clone formation, followed by auxin and cytokinin treatments and tracking of secondary LRP emergence. Our results show that secondary LRPs undergo cell fate transitions similar to those of primary LRPs: auxin promotes their emergence, while cytokinin promotes their arrest and transition toward cambium identity (Supplemental Figure 7). These findings indicate that XPP cells in mature LRs exhibit cell fate dynamics comparable to those in the primary root.

All together, our findings revealed that the LRPs, a derivative of the XPP cell lineage, display cell fate plasticity. When LRPs enter arrested state, whether under normal conditions or due to cytokinin treatment, they undergo a transition to acquire cambium identity. This transformation enables them to contribute to root secondary growth, thereby serving as an additional source for cambium, alongside the cambium-fate XPP cells, from their circumferential position in the vasculature.

LRP arrest occurs before root meristem identity is established

Based on the morphology of LRPs that had lost *DR5:erRFP* expression in 5-day-old roots, we inferred that LRP arrest occurs at early developmental stages (Supplemental Figure 6B). However, the precise stage at which an LRP becomes arrested remains unclear. One potential approach to determine this would be through live imaging. However, this method is time consuming, low throughput, and highly dependent on subjective morphological assessment. Therefore, we sought an alternative strategy to determine the developmental stage of arrested LRPs at the molecular level, rather than relying solely on morphology.

To this end, we returned to the lineage tracing method. We selected a series of LRP-stage-specific promoters, including *pGATA23,* active from founder cells to stage III/IV (De Rybel et al., 2010); 1.5 kb *PLETHORA7* (*PLT7*), an LRP-specific promoter showing expressing from stage I (Du and Scheres, 2017); *SCARECROW* (*SCR*), *PLT2*, and *PLT4*, root meristem markers active from stages III–IV onwards (Du and Scheres, 2017); and *WEREWOLF (WER)*, expressed in the later stages of emerging LRPs (Du and Scheres, 2017). We generated inducible promoters of them and used them to drive expression of CYCB1;1-CRE in the background of *35S-loxp-erGUSpYFP*. In T1 generation, 4-day-old seedlings were transferred to the estradiol-containing medium to induced YFP clones (Figure 4A). We then quantified the ratios of arrested LRP clones with YFP labeling to the total YFP clones. We found that for the transgenic lines carrying inducible promoter *pGATA23:XVE* and *pPLT7:XVE*, nearly 35% and 40% YFP clones, respectively, failed to emerge out (Figure 4B). In contrast, for the transgenic lines with root meristem inducible promoters, the ratio is much lower, especially for the *pWER:XVE*. Together with the results from the iLR Tracker and the LR Tracker, which rely on *pHB53* promoter expressing from stage I onwards, showing that about half of LRPs become arrested (Figures 2C, 4C, and 4D), we conclude that LRP arrest primarily occurs before establishment of root meristem identity. Given that root meristem regulators are mostly expressed at stage III/IV (Du and Scheres, 2017), therefore, it is likely that LRP arrest occurs at the stage I/II. This conclusion is further supported by a previous study showing that excised LRP with at least 3–5 layers can develop autonomously into LRs (Laskowski et al., 1995).

Cambium regulators do not control the cell fate of LRPs

Given that most cambium regulators are not expressed in developing LRPs (Figure 3), that cambium identity in arrested LRPs emerges after the loss of auxin signaling (Supplemental Figure 6B), and that LRP arrest likely occurs at early developmental stages during primary root growth (Figure 4A and 4B), these observations suggest that cambium regulators do not play a role in determining the cell fate of LRPs. To test this hypothesis, we used CRISPR-Cas9 to generate mutations in two cambium regulators in the LR Tracker background: *LBD4*, which is expressed in LRPs, and *PXY/TDR*, a key cambium regulator with relatively strong and specific expression in XPP cells just above the root tip, where LRP initiation occurs (see below, Supplemental Figure 10B). In the resulting *lbd4* and *pxy* mutants, the proportion of arrested LRPs was comparable to that of the WT (Figure 4C). Furthermore, auxin signaling reporter dynamics in developing LRPs of the strong cambium mutant *lbd3;4;tdr;wox4* were similar to those in the WT, with approximately half of the LRPs gradually losing their auxin signaling maximum over time (Supplemental Figure 4A). Consistently, quantification of emerged LR distribution in 10-day-old roots of cambium-related mutants showed no increase of LR numbers compared with WT (see below, Supplemental Figure 12D). Considering that cytokinin-induced depletion of auxin signaling in LRPs occurs more rapidly than the upregulation of cambium regulator expression (Supplemental Figure 6C and 6E), our findings collectively suggest that LRP arrest, cambium identity acquisition in arrested LRPs, and cambium regulators mediated secondary growth are spatiotemporally separated. Therefore, cambium regulators do not contribute to the cell fate determination of LRPs under either normal or cytokinin-treated conditions.

Endogenous cytokinin signaling control the cell fate of LRPs

It has been reported that reduced cytokinin levels, either by mutating *ISOPENTENYL TRANSFERASES* (*IPT*s), the rate-limiting enzymes in cytokinin biosynthesis or by overexpressing

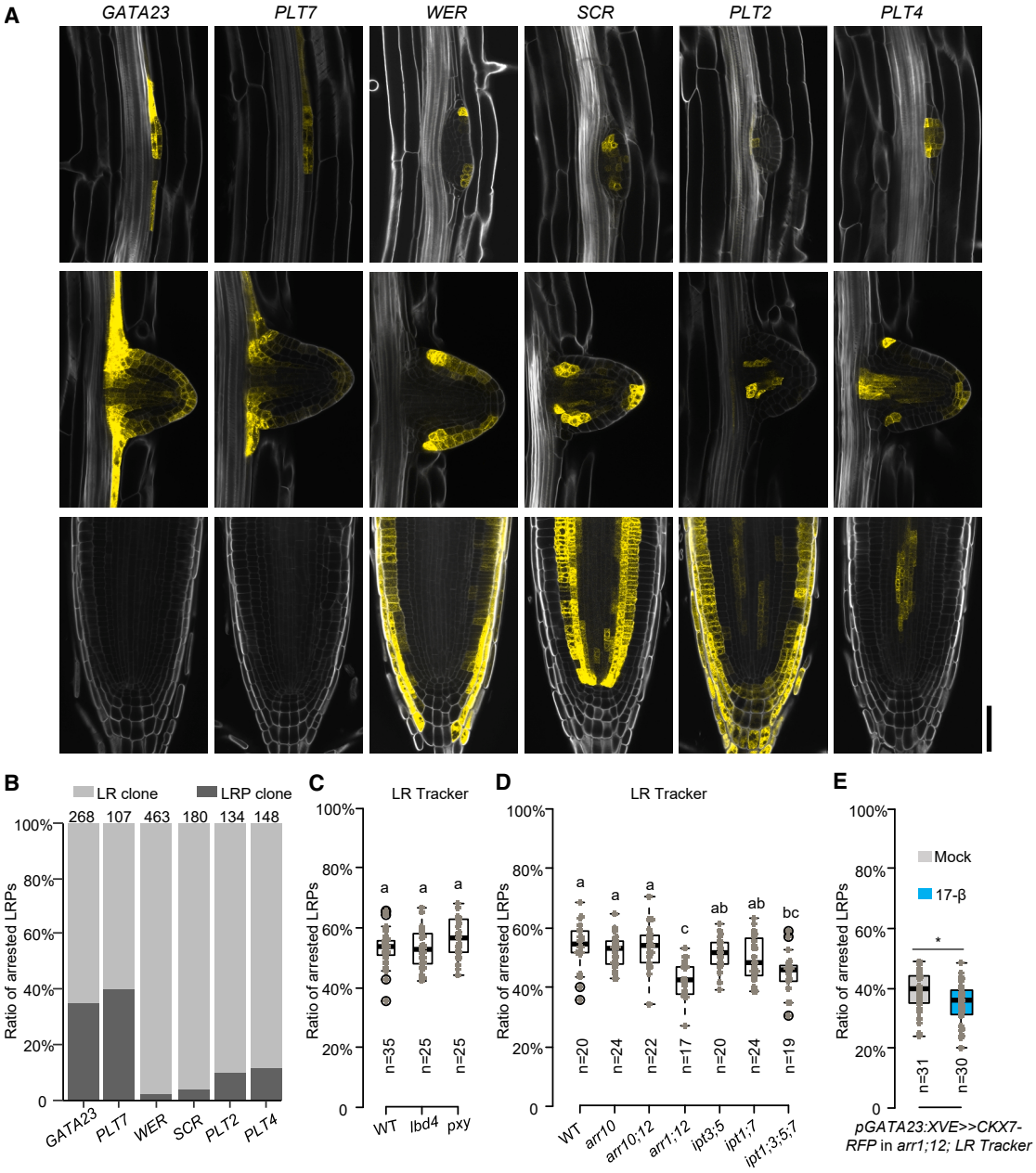

Figure 4. Determining the developmental stage at which LRPs become arrested and factors affecting LRP arrest

(A) LRPs primarily become arrested before root meristem identity is established. Various inducible promoters were used to drive CRE-CYCB1;1 expression in the *35S:loxP-erGUSpYFP* background. T1 generation seedlings were analyzed. Four-day-old seedlings grown on ½GM were transferred to induction medium for 6 days, after which YFP clones were induced in LRPs (upper panel) and LRs (middle panel) in the transferred root region (the root region growing on ½GM before transfer), or in the newly grown root tips (lower panel) for some transgenic lines. The unemerged LRPs were regarded as arrested LRPs. Note that not all LRPs could be marked, as some may have become arrested before induction. Scale bar, 50 μm.

(B) Ratio quantification of arrested LRPs after 6 days of growth on induction medium. Data are presented as the percentage of YFP-labeled LRP clones relative to the total number of clones (YFP-labeled LRs + LRPs). Numbers indicate total clones observed under each inducible promoter from 19 to 66 individual roots.

(C) Mutation of cambium regulators LBD4 and PXY/TDR resulted in a similar ratio of arrested LRPs compared to the WT control (LR Tracker).

(D and E) Reducing endogenous cytokinin levels or cytokinin signaling led to a lower proportion of arrested LRPs. Six-day-old seedlings grown on ½GM or mock/induction medium were transferred to fresh ½GM for another 6 days before quantification. The YFP-labeled LRP clones and LR clones were quantified from the transferred root zone, where the unemerged LRPs were considered as arrested LRPs. The ratio of arrested LRPs was calculated as the number of YFP-marked LRPs relative to the total clone numbers (YFP-marked LRs + LRPs)

(C–E) Significant differences **(C** and **D)** were identified at $\alpha = 0.05$ using one-way ANOVA followed by Tukey's HSD post hoc test, with different letters indicating statistically distinct groups. A two-tailed Welch's *t*-test was performed (*$p < 0.05$; **E)**. The "n" indicates the number of samples analyzed **(C–E)**.

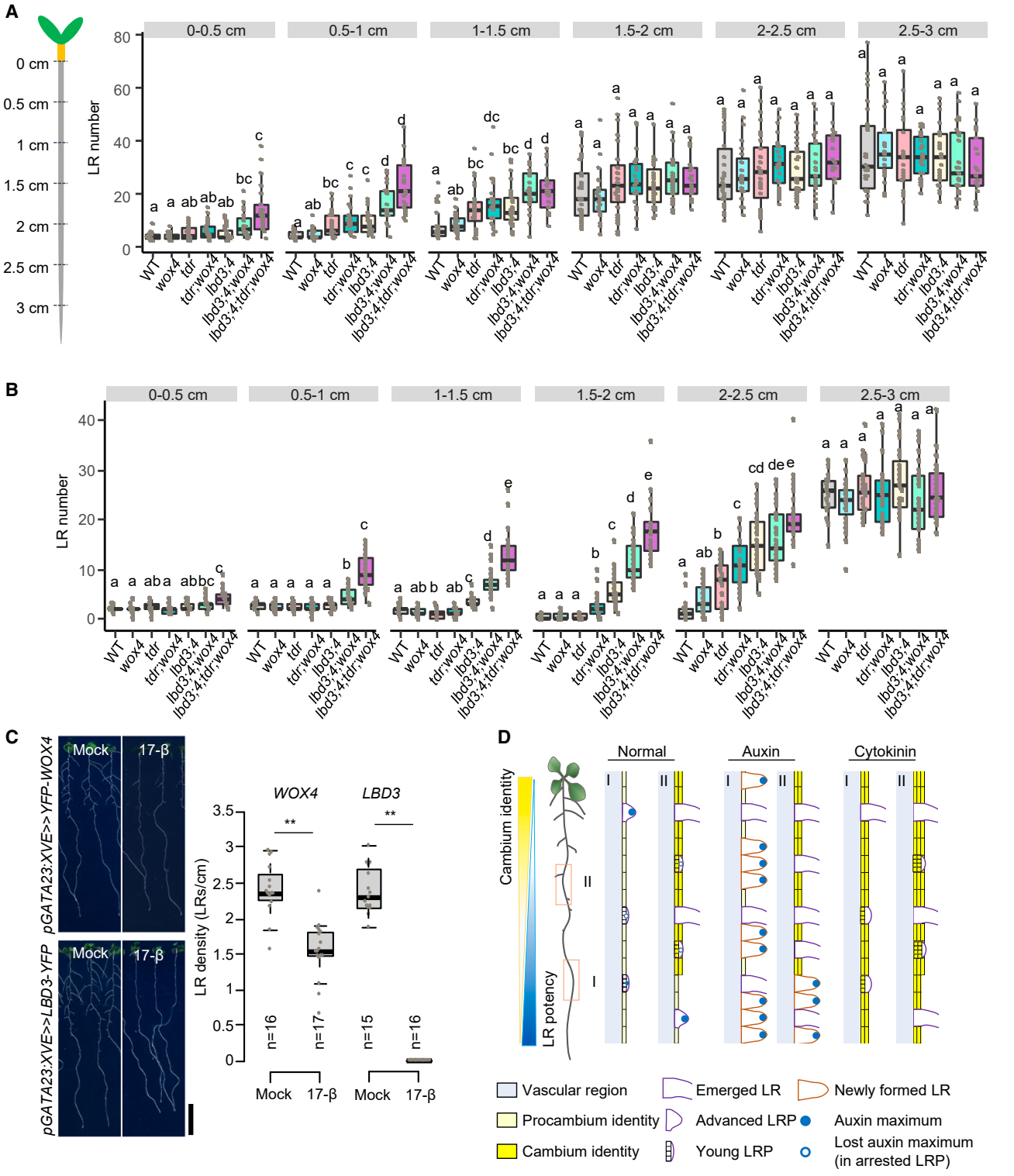

Figure 5. Cambium regulators shape the LR potency

(A and **B)** Auxin-induced LR potency characterization of WT roots and cambium defective mutant roots. Seven-day-old roots grown on standard ½GM from distinct genotypes were treated for 3 days with 5 μM NAA without **(A)** or with **(B)** a 2-day 1-μM BAP pretreatment. The left schematic **(A)** shows the strategy used to quantify emerged LRs in each root zone. Note, *lbd3;4* and *lbd3;4;wox4* **(B)** exhibited a significant increase in LR induction in the root zone 1–1.5 cm and 0.5–1 cm, respectively, where frequent cambium-like cell divisions occurred (Supplemental Figure 14). A total number of 20–35 root samples were used for quantification in each genotype. Significant differences, indicated by different letters, were determined at an alpha level of 0.05 using a one-way ANOVA with either Tukey's post hoc test (for equal homogeneous variance) or Tamhane's post-test (for unequal variance).

(legend continued on next page)

the cytokinin oxidase gene *CKX1*, increases LR and LRP density (Chang et al., 2013). A similar effect is observed when components of the cytokinin signaling pathway are disrupted (Chang et al., 2013). In contrast, increased cytokinin levels block LRP initiation and development (Li et al., 2006; Laplaze et al., 2007; Chang et al., 2013). Using the iLR Tracker and cambium reporters, we demonstrated that cytokinin treatment promotes LRP arrest and the transition of cell identity to cambium (Figures 2C and 3).

To study whether endogenous cytokinin signaling regulates LRP cell fate, we generated CRISPR-Cas9 knockout mutants in the LR Tracker background by targeting key components mediating cytokinin signaling and cytokinin biosynthesis. These include type-B *ARABIDOPSIS RESPONSE REGULATORS* (*ARRs*), *ARR1*, *ARR10*, and *ARR12* as well as cytokinin biosynthesis gene *IPT1*, *IPT3*, *IPT5*, and *IPT7*. The combination with LR Tracker allowed us to directly visualize arrested LRPs and quantify the ratio of arrested LRPs to the total number of LRs/LRPs in the mutants. A total of six mutant combinations were obtained, *arr10*, *arr10;12*, *arr1;12*; *ipt3;5*, *ipt1;7*, and *ipt1;3;5;7*. Among these mutants, *arr1;12* and *ipt1;3;5;7* exhibited a significantly lower ratio of arrested LRPs, indicating that more LRPs successfully develop into LRs (Figure 4D). These results indicate that endogenous cytokinin signaling indeed plays a role in regulating the cell fate of LRPs, in addition to its known inhibitory functions in LRP initiation and development. An examination of cytokinin spatial distribution in roots revealed high levels of active cytokinin in the LRP initiation zone (Bielach et al., 2012), suggesting that endogenous cytokinins in this region likely play a key role in determining LRP cell fate.

Furthermore, when cytokinin levels were conditionally reduced in the *arr1;12*; *LR Tracker* background by expressing the cytokinin oxidase gene *CKX7* (Köllmer et al., 2014; Ye et al., 2021) under the *pGATA23:XVE* promoter, a slightly but significantly lower ratio of arrested LRPs was observed. However, a large proportion of LRPs remained arrested (Figure 4E). This observation suggests that additional unidentified factors also contribute to the cell fate determination of LRPs.

Cambium regulators shape LR potency

The findings above demonstrated the fate plasticity of LRPs by reversing LRP identity to cambium identity, under normal conditions or by cytokinin treatment. Previous reports indicate that cambium-fate XPP cells maintain the competence to form new LRs when stimulated by auxin, but the competence decreases in the segmented upper region of 10-day-old roots growing on medium containing 10 μM NPA (Dubrovsky et al., 2008, 2011). We therefore utilize the auxin-induced LR potency as a proxy to evaluate the fate plasticity of cambium-fate XPP cells. To characterize LR potency in an intact root at a higher resolution, we used the LR Tracker for this purpose with various supplemented auxin levels. We observed that 50 nM NAA triggered *de novo* LR formation (i.e., LR formation from the cambium-fate XPP cells) in the region primarily near the root tip; while above this region, only the development of existing LRs/LRPs were affected (Supplemental Figure 8A and 8B). When supplying 1 μM NAA, after a 3-day induction, *de novo* LR formation was observed in a broader root region in the lower part of the root. In the upper part of the root, LR initiation seemed to occur as well; however, in most cases, it did not lead to LR outgrowth (Supplemental Figure 8A and 8B). We then increased NAA level to 5 μM and found massive and continuous *de novo* LR formation in the root region from about 1.5 cm below the hypocotyl toward the root tip, while the upper root region (about 1 cm) remained less responsive despite such a high level of auxin (Supplemental Figure 8A and 8B). Decreased auxin-induced LR potency as root matures was also observed by a detailed quantification of LR distribution in WT roots after a 3-day 5-μM NAA treatment (Supplemental Figure 8C). These results indicated that the fate plasticity of cambium-fate XPP cells, as indicated by LR potency, is determined not only by the supplied auxin levels but also by the status of root maturity.

We also developed an XPP cell lineage tracing system by using an XPP-specific inducible promoter (Andersen et al., 2018) driving CYCB1;1-CRE expression. With this system, we confirmed first that the NAA-induced, newly formed LRs originated from XPP cell lineage, and second, the LR potency decreased as root matures (Supplemental Figure 8D). Cytokinin biosynthesis mutant *ipt1;3;5;7*, which lacks cambium activity in the root and hypocotyl (Matsumoto-Kitano et al., 2008), exhibited exceptional LR potency, with auxin treatment triggering LR induction along the entire root length (Supplemental Figures 8C and 9), thus confirming a previous finding (Bielach et al., 2012). The decreased LR potency within the WT roots and the differences in LR potency observed between WT and *ipt1;3;5;7* mutant roots suggest the presence of regulators associated with cytokinin-induced secondary growth governing LR potency as well as the fate plasticity of cambium-fate XPP cells.

We proceeded to investigate the mechanism underlying our observations. Since cambium-fate XPP cells are destined for cambium formation, we proposed that the gradual acquisition of cambium identity may account for their decreased fate plasticity. To test this, we first performed serial cross-sections to 7-day-old WT roots to explore the relationship between LR potency and status of maturity within XPP cell lineage. Statistical analysis showed that cambium activation (i.e., initiation of the periclinal cell divisions) predominantly occurred within the region spanning 1–1.5 cm below the hypocotyl of 7-day-old seedlings. Above this region, cambium is typically fully activated, while below it, cambium activation rarely occurred (Supplemental Figure 9A and 9B). This gradual cambium activation pattern aligned well with LR potency along the root: extensive LR induction was observed below this region (Figure 5A and Supplemental Figures 8C and 9), while LR induction was limited above it.

(C) Key cambium regulators are sufficient to inhibit LR development. The emerged LRs were quantified in each overexpression line after 8 days of germination on mock or induction medium. *n*, number of independent roots analyzed. Two-tailed Welch's *t*-test was performed. $^{**}p < 0.01$. Individual data points are plotted as gray dots **(A–C)**. Scale bar, 1 cm.

(D) A simplified model illustrating how auxin and cytokinin balance cambium and LR fates of XPP cell lineage. While auxin promotes LR fate acquisition, cytokinins facilitate cambium fate acquisition.

We then analyzed the expression dynamics of cambium regulator genes within XPP cell lineage in 7-day-old roots. Our analysis revealed a gradient expression pattern of cambium regulators within cambium-fate XPP cells increasing toward the shoot, except for *PXY/TDR* (Supplemental Figure 10A), which displayed an opposite trend (Supplemental Figure 10B). Reporter analysis indicated that once they exit the root apical meristem, cambium-fate XPP cells gradually acquire procambium identity before transforming into cambium when cambium activation occurs, similar to the developmentally arrested LRPs (Figures 2F, 3, and Supplemental Figure 6B). The procambium identity can be conversely reverted to LR identity upon auxin treatment. For example, the expression of cambium regulator genes was clearly visible within the region 1.5–2 cm below the hypocotyl, where cambium was not yet activated, and auxin application is able to induce massive LR formation in this zone (Supplemental Figures 8C, 9, and 10A). We also tracked this identity transition through a time-course reporter analysis using LR reporters *pGATA23:nlsGFPGUS*, *pLBD16:erYFP*, and a cambium reporter *pPXY:erYFP*, each crossed with *DR5:erRFP* to visualize auxin response dynamics. Following 5 μM NAA treatment, transcriptional activity of *DR5*, *pGATA23*, and *pLBD16* was rapidly induced along XPP cells within 4 h, with continued increase observed alongside new LRP initiation from 8 h onward. In contrast, in the young XPP cells without cambium activation, *pPXY* exhibited a gradual decline in transcriptional activity during this process (Supplemental Figure 11). However, when sustained expression of cambium regulators finally cause cambium activation, the reinforced cambium identity appears to inhibit auxin-induced LR formation (Supplemental Figures 8C, 9A, 9B and 10A).

To further explore the effects of cambium regulators on LR potency, we investigated cambium mutants and examined the relationship between their cambium activation and LR potency. For this purpose, we focused on mutants related to *PXY/TDR*, *WOX4*, *LBD3*, and *LBD4*, which are known critical cambium regulators (Wang et al., 2023) and loss-of-function mutants of them show gradual increase in the severity of cambium activation defects from single, double, triple, to quadruple mutants, as indicated from serial cross-sections of these mutants (Supplemental Figure 9A and 9B). While the mutants showed similar primary root length as WT and LR distribution after mock treatment (Supplemental Figure 12), we again discovered a strong correlation between cambium activation defects and LR potency along the root after auxin treatment (Figure 5A, Supplemental Figure 9). For instance, the most severe mutant combination, *lbd3;4;tdr;wox4*, which exhibited no cambium activation in 7-day-old roots, showed efficient LR induction along the entire root length (Figure 5A, Supplemental Figure 9). Therefore, cambium regulators shape the LR potency and cell fate plasticity of cambium-fate XPP cells along the root.

Next, we asked whether any of the cambial regulators are sufficient to prevent LR formation. We induced ectopic overexpressions of cambium regulator genes in the early LRP and the young root region by using the *GATA23* inducible promoter. For this purpose, we included PXY/TDR, WOX4, LBD3, LBD4, LBD11, ANT, and the HD-ZIP III transcription factor ATHB8, which acts downstream of auxin signaling in determining vascular stem cell organizer (Smetana et al., 2019). Ectopic expression analysis revealed that all these tested cambium regulators inhibited LR development to various degrees (Figure 5C and Supplemental Figure 13A and 13B). PXY/TDR expression alone had no obvious effects on LR development, however, when combined with the treatment of its ligand, TRACHEARY ELEMENT DIFFERENTIATION INHIBITORY FACTOR (TDIF) (Ito et al., 2006), a clear inhibitory effect was observed (Supplemental Figure 13A and 13B). Over-expressions of WOX4, LBD3, and LBD4 appeared to show stronger LR development inhibition compared with other cambium regulators, in line with broader LR potency in their corresponding mutants. Therefore, the inhibitory effects of cambium regulators on LR development explain the restriction of LR potency exerted by cambium activation within XPP cells. Despite the clear inhibitory effect on LRP development, overexpression of *LBD3* and *LBD4* led to an enhanced auxin signaling response in developing LRP following induction (Supplemental Figure 13C–13E). This was accompanied by ectopic anticlinal cell divisions in XPP cells, suggesting that *LBD3* and *LBD4* primarily exert their inhibitory roles at post-initiation stages. For different cambium regulators, it is possible that they inhibit LR development in a different manner.

Overall, our results indicated that the procambium identity within XPP cells can be reverted to LR identity stimulated by high levels of auxin, further highlighting the fate plasticity of cambium-fate XPP cells. However, gradual elevation of cambium regulator expression within XPP cells, especially TDIF-PXY/TDR, WOX4, LBD3, and LBD4, will lead to cambium activation and identity reinforcement, thereby these cambium regulators serve as limiting factors for the cell fate plasticity of cambium-fate XPP cells.

Cambium regulators are required for cytokinin-mediated inhibition of lateral root potency

The previous findings have shown that pretreatment with cytokinin or expressing a cytokinin biosynthesis gene in the XPP cells diminishes the effectiveness of auxin induced LR formation, suggesting the compromised fate plasticity within cambium-fate XPP cells in the presence of cytokinin. However, the underlying mechanism is unknown (Li et al., 2006; Laplaze et al., 2007). Given that cytokinins prompt premature cambium activation (Ye et al., 2021) and they promote LRP to cambium identity transition (Figure 3, Supplemental Figure 7), we formulated a hypothesis that cytokinins impede auxin-induced LR potency by facilitating cambium activities within XPP cells. To investigate this hypothesis, we conducted serial sections in the WT and cambium mutant roots following cytokinin treatment and quantified cambium activation events within XPP cell lineage (Supplemental Figure 14). Within the 0–2.4 cm root region below the hypocotyl, activation of cambium in XPP cells was evident in the WT root, which again correlated with the limited LR induction by auxin within this region (Figure 5B, and Supplemental Figure 14). Notably, cambium mutants exhibited an expanded auxin-induced LR potency subsequent to cytokinin pretreatment, with the *lbd3;4;tdr;wox4* mutant displaying the most pronounced LR potency (Figure 5B and Supplemental Figure 14). Interestingly, different from the WT, *lbd3;4* and *lbd3;4;wox4* demonstrated a significant increase in LR induction even from the root region where a frequent cambium-like cell divisions occurred (Figure 5B and Supplemental Figure 14). This finding suggests

that not cambial cell divisions themselves, but reinforced cambium identity rendered by key cambium regulators, serve as a limiting factor restricting LR potency. We also observed that cytokinin pretreatment reduced the number of induced LRs, particularly in cambium-defective mutants lacking one or two cambium regulators (Figure 5A and 5B). This is likely because these mutants retain residual cambium activity, enabling cytokinin to activate cambial divisions (Supplemental Figure 14A and 14B), which in turn inhibits auxin-induced LR formation. Together, our results indicated that cytokinins play their inhibitory roles on auxin-mediated LR potency via promoting cambium activity. During this process, key cambium regulators are involved.

DISCUSSION

The developmental plasticity of plants ensures their ability to sustain growth in response to fluctuating environments. In this study, we delved into the fate plasticity of XPP cell lineage with respect to their dual cell fates. First, we developed novel LR-tracing systems, iLR Tracker and LR Tracker, to enhance LR/LRP visualization and demonstrated their broad applicability in various conditions. In contrast to cambium-fate XPP cells, developing LRPs exhibit distinct morphological features characterized by short cell walls and a domed shape, attributed to patterned cell divisions. Traditional quantification of LRs/LRPs rely heavily on standard wide-field microscopes (Malamy and Benfey, 1997), which could lead to the oversight of LRPs in root zones undergoing secondary growth or positioned non-orthogonally to the light path. To address this limitation, researchers often use LR reporters, albeit with drawbacks such as nonspecific or transient, stage-specific expression and faint or absent expression in arrested LRPs (Figure 1F). Our newly developed systems, which specifically, strongly, and permanently marks LRPs post-recombination, enable direct visualization of LRs/LRPs in intact roots under a fluorescence stereo microscope, therefore facilitating convenient and high-throughput LR-related quantification. In addition to the *35S:loxP-erGUSpYFP* construct used in this study, we also provided five additional vectors for the research community by replacing 35S promoter with other two frequently used constitutive promoter UBIQUITIN10 (Norris et al., 1993) and HTR5 (Ingouff et al., 2017) or by changing the coding sequence of YFP to RFP (Figure 1B).

Using the iLR Tracker and cambium reporters, we revealed that approximately half of the LRPs in the mature root zone became arrested and eventually acquired cambium identity under our growth conditions (Figures 2C, 2F and 5D). Furthermore, we demonstrated that cytokinins promoted arrest of young LRPs and the transition from LRP identity to cambium identity (Figures 2B, 2C, 3 and 5D). Compromised cytokinin levels or cytokinin signaling causes reduced proportion of arrested LRPs (Figure 4C), consistent with their established inhibitory roles in LR development (Li et al., 2006; Laplaze et al., 2007; Marhavý et al., 2011; Bielach et al., 2012; Chang et al., 2013, 2015; Jing and Strader, 2019). The occurrence of LRP arrest appears to be independent of cambium regulators, as most of these genes are not expressed in active LRPs (Figure 3). Furthermore, the acquisition of cambium identity in arrested LRPs takes place after the loss of the auxin signaling maximum (Supplemental Figure 6B). Lineage tracing further revealed that LRP arrest occurs prior to the establishment of root meristem identity (Figure 4A and 4B), most likely at stage I/II, before the onset of secondary growth. This explains why mutants of cambium regulators show similar numbers of LRs and comparable ratios of arrested LRPs relative to WT (Figure 4C, Supplemental Figure 12D).

A well-established auxin signaling maximum is believed to play a crucial role in the development of LRP (Benková et al., 2003; Bielach et al., 2012). Our results suggest that LRP arrest might result from a failure to maintain this auxin maximum. Supporting this, transiently disrupting auxin transport signaling or downstream target involved in LR development promotes arrest of LRPs and transition to cambium fate (Supplemental Figure 4B–4F). And supplementing low concentrations of auxin to a 4-day-old root was effective in stimulating the emergence of most LRPs, while higher concentrations of auxin could awaken arrested LRPs in a 7-day-old root (Figure 2B, 2C, and Supplemental Figure 5A). However, as the root matures, the capacity of auxin to reactivate arrested LRPs diminishes (Supplemental Figures 5A, 8A, and 8B), because these LRPs have already acquired and reinforced their cambium identity (Figures 2F and 5D).

In this study, expression analysis of cambium regulators revealed a gradual acquisition of cambium identity of cambium-fate XPP cells, as root matures (Figure 5D and Supplemental Figure 10A). When expressions of cambium regulator genes reach a threshold level, cambium activation occurs. Even though in this study only XPP cell lineage was followed, it is likely that in the vascular region, procambium activation to cambium occurs in a similar manner. With the LR Tracker, cambium, and LR reporters, we showed that the procambium identity within XPP cells could be reverted to LR identity by auxin treatment (Figure 5A, Supplemental Figures 8–11). When cambium activation occurs, the cells in XPP lineage become less responsive to auxin-induced LR formation, likely due to their strengthened cambium identity, boosted by the key cambium regulators PXY/TDR, WOX4, LBD3, and LBD4. Supporting this, induction of these regulators in early LRP cells strongly inhibited LR development, and the corresponding knockouts displayed expanded LR potency (Figure 5, Supplemental Figures 9C, 13A, and 13B). It is possible that other cambium regulators also contribute to this process, such as ATHB8, whose ectopic expression showed strong LR development inhibition (Supplemental Figure 13A and 13B).

It has been shown that auxin application fails to rescue the defect in LR initiation when a cytokinin biosynthesis enzyme, IPT, is expressed in XPP cells or following cytokinin pretreatment (Li et al., 2006; Laplaze et al., 2007). In this study, our data showed that cytokinin pretreatment lowers LR potency via premature cambium activation within XPP cells in a process requiring at least PXY/TDR, WOX4, LBD3, and LBD4 (Figure 5B, 5D and Supplemental Figure 14). This represents another pathway inhibiting LR development, which is likely different from their direct inhibitory effects on LR development via modulating PIN1-mediated auxin transport (Marhavý et al., 2011). Although these cambium regulators are not involved in controlling cell fate determination of LRPs under normal conditions, our findings indicate that they contribute to shaping LR potency

when auxin levels change. A prior study indicated that while LR formation is the predominant response to auxin treatment in 4-day-old seedlings, for 6-day-old seedlings, auxin treatment induces periderm formation instead, in the mature part of the root (Xiao et al., 2020). This phenomenon has been observed earlier as well (Dubrovsky et al., 2011). This dual role of auxin can potentially be explained by our findings. Our data suggest that once accumulation of cambium regulators establishes cambial identities in XPP and the remaining pericycle cells, then auxin has a new role in promoting further cambial development and root maturation. This, in turn, limits the cell fate plasticity of XPP lineage to form LRs. In conclusion, our findings demonstrated the control of cell fate plasticity of XPP lineage in *Arabidopsis* roots and elucidated how plant hormones auxin and cytokinin influence root architecture and secondary growth through balancing LR fate and cambium cell fate of XPP cells. This regulation may reflect a biological strategy to balance water and nutrient uptake with the mechanical support in the natural environment. Although this study focused on the roles of auxin and cytokinin in regulating the cell fate plasticity of LRP and cambium-fate XPP cells (which we collectively name as XPP cell lineage), it is likely that various internal and external cues influencing LRP initiation and post-initiation development also contribute to such plasticity.

METHODS

Vector construction and *Arabidopsis* transformation

To generate the *pXPP:XVE* inducible promoter, a 2.5-kb XPP-specific promoter (Andersen et al., 2018) was cloned into the first box entry vector *1R4a-ML-XVE* (Siligato et al., 2016) by restriction enzyme digestion and ligation. To facilitate the construction of inducible promoters, we modified the *1R4a-35S-XVE* vector ("a" denotes ampicillin resistance) by adding Asc I and Fse I restriction enzyme sites flanking the *35S* promoter sequence through omega PCR (Chen et al., 2013; Wang et al., 2020), yielding the *1R4a-AscI-35S-FseI-XVE* vector. Subsequently, a 1.1-kb *GATA23* promoter sequence was introduced by replacing the *35S* promoter via digestion and ligation. The *1R4a-35S-XVE* vector was further modified by incorporating multiple cloning sites flanking the *35S* promoter using omega PCR (Chen et al., 2013; Wang et al., 2020) to generate a universal intermediate vector, *1R4a-MCS-35S-MCS-XVE*. A 2-kb *HB53* promoter sequence was first integrated into the first box donor vector pDONR1R4z ("z" denotes zeocin resistance) via BP reaction, to produce the *1R4z-pHB53* entry vector. The HB53 promoter sequence was also cloned into the *1R4a-MCS-35S-MCS-XVE* vector through digestion and ligation to produce *1Ra-pHB53-XVE*. Promoter sequences of *PLT2*, *PLT4*, and *PLT7* were cloned into the *1R4a-MCS-35S-MCS-XVE* vector in a similar way. The RFP coding sequence from the published *221z-erGUSpRFP* entry vector ("z" denotes zeocin resistance) (Mäkilä et al., 2023) was replaced with YFP coding sequence via omega PCR (Chen et al., 2013; Wang et al., 2020), to generate *221z-erGUSpYFP*.

A longer version of *35S* promoter (Hunter et al., 2019) and a 2-kb *HTR5* promoter (Ingouff et al., 2017) were used to substitute for the shorter version of *35S* promoter in the published *1R4z-35S-Loxp* entry vector (Smetana et al., 2019) through omega PCR (Chen et al., 2013; Wang et al., 2020), for the generation of *1R4z-p35S$_{long}$-loxP* and *1R4z-pHTR5-loxP*, respectively. To avoid misunderstanding, the *35S$_{long}$-loxP* in this paper is presented as *35S-loxP*. The construction of the *1R4z-pUBQ10-loxP* vector was performed with a different strategy. Initially, multiple cloning sites were introduced into the flanking sites of the *35S* promoter of the published *1R4z-35S-loxP* entry vector (Smetana et al., 2019) via omega PCR (Chen et al., 2013; Wang et al., 2020) to produce a common intermediate vector *1R4z-MCS-35S-MCS-loxP* entry vector, which was followed by the replacement of the *35S* promoter with a 2-kb *UBQ10* promoter sequence through digestion and ligation.

All binary expression constructs were generated through multisite gateway LR reactions. The promoters *1R4a-pGATA23-XVE*, *1R4a-pHB53-XVE*, *1R4a-pHB53*, *1R4a-pPLT2-XVE*, *1R4a-pPLT4-XVE*, *1R4a-pPLT7-XVE*, *1R4a-pSCR-XVE*, and *1R4a-pWER-XV* in the first boxes, recombinase coding sequences 221z-CRE (Smetana et al., 2019) and *221a-CYCB1;1-CRE* in the second boxes (Smetana et al., 2019), and the terminator *2R3a-nosT* in the third box were combined into the destination vector *FRm43GW* (Wang et al., 2020). The first box entry vectors *1R4z-35S-loxP*, *1R4z-pHTR5-loxP*, and *1R4z-pUBQ10-loxP*, second box entry vectors *221z-erGUSpYFP* and *221z-erGUSpRFP* (Mäkilä et al., 2023), and the third box entry vector *2R3a-nosT* were integrated into the destination vector *pBM43GW* (Karimi et al., 2002). In this study, we tested the *35S-loxP-erGUSpYFP* construct by first transforming it into Col-0 background. Then in T2 generation, 15 independent, likely single insertion lines (as indicated by Mendelian segregation ratio) were screened and transformed with *pGATA23:XVE>>CRE*. The most suitable *35S:loxP-erGUSpYFP* line was selected based on performance (i.e., consistent and non-leaky clone formation) with *pGATA23:XVE>>CRE*, and that line (without *pGATA23:XVE>>CRE*) was used as the background for subsequent studies.

The reporter lines used in this study, *DR5:erRFP* (Siligato et al., 2016), *pPXY:erYFP* (Smetana et al., 2019), *pWOX4:erYFP* (Smetana et al., 2019), *pLBD3:erYFP* (Ye et al., 2021), *pLBD4:erYFP* (Ye et al., 2021), *pANT:erRFP* (Mäkilä et al., 2023), *pWOX5:erGFP* (Blilou et al., 2005), *gPLT1YFP* (Mähönen et al., 2014) have been published before. A 2-kb promoter sequence of *PER15* (Xiao et al., 2020) and a 4.5-kb promoter for LBD16 were cloned into the first box donor vector *1R4z-BsaI-ccdB-BsaI* (Mäkilä et al., 2023) via Golden Gate Cloning to produce *1R4z-pPER15 and 1R4z-pLBD16*. The first box entry vectors *1R4z-pPER15*, *1R4a-pPLT2* (Mähönen et al., 2014), *1R4z-pLBD16*, *1R4a-pHB53*, second box entry vectors *221z-erYFP*, 221z-*erRFP* (Siligato et al., 2016), and *2R3a-nosT* (Siligato et al., 2016) were combined into the destination vector *pHm43GW* or *pBm43GW* (Karimi et al., 2002) to generate the respective reporter construct. The constructs *pHB53:XVE>>axr3-1-RFP* and *pHB53:XVE>>axr3-1-YFP* were generated by combining three modules, *1R4a-pHB53-XVE* (first box), *221z-axr3-1* (second box) (Smetana et al., 2019), and either *2R3z-4xgly-YFP* or *2R3z-4xgly-RFP* (third box) (Siligato et al., 2016), into the destination vector *pF7m34GW* (Wang et al., 2020). To create *221z-gLBD16-SRDX*, we fused the SRDX coding sequence to the genomic sequence of LBD16 using a two-step PCR approach. In the first round, we used a forward primer with a full-length attB1 adapter and a reverse primer containing the SRDX sequence. In the second round, the same forward primer and a new reverse primer with a partial SRDX sequence and full-length attB2 adapter were used, with the first PCR product as the template. The final PCR product (*attB1-gLBD16-SRDX-attB2*) was cloned into the donor vector *pDONR221z* via BP recombination, generating *221z-gLBD16-SRDX*. Finally, to produce *pHB53:XVE>>gLBD16-SRDX*, we assembled *1R4a-pHB53-XVE*, *221z-gLBD16-SRDX*, and *2R3a-nosT* (Siligato et al., 2016) into the destination vector *pFG7m34GW* (Wang et al., 2020).

Constructions of *221z-ANT* and *221z-ATHB8* entry vectors were described elsewhere (Smetana et al., 2019). The coding sequences of *LBD3*, *LBD4*, and *LBD11* without stop codons and the genomic sequence of *PXY/TDR* with the stop codon were cloned into the second box donor vector *221z-BsaI-ccdB-BsaI* (Wang et al., 2020) through Golden Gate Cloning. The construction of *221z-BsaI-ccdB-BsaI* was performed as previously described (Wang et al., 2020). The coding sequences of *YFP* and *WOX4* were initially separately amplified in the first round PCR and then combined into a fusion of *YFP-WOX4* through

a second round overlapping PCR, which was followed by a subsequent BP reaction to produce the *221z-YFP-WOX4* entry vector. For cambium regulator ectopic expression analysis, the inducible promoter *1R4a-pGATA23-XVE*, respective cambium regulator genes, and *2R3a-nosT* (for *PXY/TDR* and *YFP-WOX4*) or *2R3a-YFP* (Siligato et al., 2016) (for other cambium regulator genes) were integrated into either *pBm43GW* (Karimi et al., 2002) or *pFRm43GW* (Wang et al., 2020) destination vectors. All constructs were transformed into *Arabidopsis* Col-0 background. For each construction, more than 10 lines were analyzed, and one representative line showing consistent expression or phenotype with others was used for further analysis. All primers used in this study are listed in the Supplemental Table 1. All constructs generated in this study are listed in the Supplemental Table 2.

The cambium defective mutants used in this study, *wox4*, *tdr*, *tdr;wox4*, *lbd3;4*, and *lbd3;4;wox4*, were published elsewhere (Ye et al., 2021). The mutant combination *lbd3;4;tdr;wox4* was produced by crossing *lbd3;4* with *tdr;wox4*.

Mutant generation by CRISPR-Cas9

To directly observe arrested LRP, CRISPR-Cas9 mutants were generated in the LR Tracker background. The previously published CRISPR construct targeting *LBD4* was used to produce the *lbd4* mutant (Ye et al., 2021). For other mutants, we employed a CRISPR-Cas9 system based on intronized Cas9 (iCas9) driven by the *RPS5A* promoter (Grutzner et al., 2021), with minor modifications to make it compatible with the Gateway cloning system. The *RPS5A* promoter and *iCas9* coding sequence were cloned into the entry vectors *1R4z-BsaI-ccdB-BsaI* (Mäkilä et al., 2023) and *221z-BsaI-ccdB-BsaI*, respectively, via Golden Gate cloning (Wang et al., 2020). The sgRNA expression cassettes were assembled using a two-step overlapping PCR method. In the first round PCR, the sgRNA promoter *AtU6-26* and scaffold were amplified separately together with the target sequences, using *pAGM55261* (Addgene #153210) (Grutzner et al., 2021) and *pHEE2E TRI* (Addgene #71288) (Wang et al., 2015) as templates. The resulting two PCR fragments were then combined into complete sgRNA expression cassettes in the second round PCR. In our Golden Gate cloning strategy, we assembled two expression cassettes. For the first cassette, we used the primer pairs PUF-TG1/PUR-XX and PSF-XX/PSR-TG1 in the first round PCR, followed by PUF-TG1/PSR-TG1 in the second round. For the second cassette, the primers PUF-TG2/PUR-XX and PSF-XX/PSR-TGR were used in the first round, followed by PUF-TG2/PSR-TGR in the second round. Here, "xx" represents the gene of interest. Two sgRNA expression cassettes were cloned into the third-box entry vector *2R3z-BsaI-ccdB-BsaI* (Wang et al., 2020) via Golden Gate cloning. The sgRNA expression cassette targeting PXY/TDR using the *AtU3b* promoter was cloned as previous described (Wang et al., 2020). The resulting entry vector containing sgRNA expression cassette was then assembled into the destination vector *pFG7m34GW*, together with *1R4z-pRPS5A* and *221z-iCas9*. All target sites were selected using CHOPCHOP (Labun et al., 2019). For *ARR12* editing, two different sgRNA targets were used. All mutants were analyzed from at least the T2 generation, with the CRISPR construct segregated out. The CRISPR construct targeting *IPT3* and *IPT5* was introduced into the *ipt1;7*;*LR Tracker* background to generate the *ipt1;3;5;7*;*LR Tracker*. All primers, constructs, and mutant genotypes are listed in the Supplemental Tables 1–3, respectively.

Plant growth and chemical treatment

Seeds were surface sterilized and stratified for 2 days at 4°C before plating on half-strength MS growth medium containing 0.5 × MS salt mixture with vitamins (Duchefa), 1% sucrose, 0,5g/L MES (pH 5.8), and 0.8% agar. Transgenic seeds were screened either under a fluorescence stereo microscope (Leica M165 FC) or on growth medium containing 20μ/ml phosphinotricin (Sigma) or 20μ/ml hygromycin (Sigma). Plates were vertically positioned in the growth chamber at 23°C with long-day settings (16 h light and 8 h dark). Stock solutions of 10 mM (NAA; Sigma), 10mM 6-benzylaminopurine (BAP; Sigma) and 10 mM 1-NPA (Sigma) were prepared in dimethyl sulfoxide (DMSO; Sigma) and diluted into required working concentrations. Aqueous 10 mM stock solution of TDIF peptides (GeneCust) was prepared and stored at −80°C and diluted to 1 μM as working concentration. 20 mM 17-β-estradiol (17-β; Sigma) was dissolved in DMSO as stock solution and diluted to 5 μM as working concentration. Potassium nitrate (Sigma), mannitol (Sigma), and sodium chloride (Sigma) were added to the growth medium to indicated concentrations. Auxin treatment in LR-tracing experiments was performed on solid growth medium with 0.8% plant agar. For LR induction experiments performed in WT and cambium defective mutants, liquid growth medium with 0.2% plant agar was used. An equal volume of DMSO solution was added to growth medium as mock treatment.

GUS staining and histological sections

GUS staining was performed as previously described (Smetana et al., 2019). Serial longitudinal sections and serial cross-sections were carried out as described previously (Kareem et al., 2016). For vibratome sections, 7-day-old root samples were first fixed in 4% paraformaldehyde solution (in 1× PBS, pH 7.2, Sigma) overnight, then rinsed twice with 1× PBS, aligned manually on a glass slide placed on ice, and cut every 0.5 cm. The segmented root samples were then embedded in 4% agar (Sigma, dissolved in 1× PBS) for subsequent vibrotome sections. Vibratome sections was carried out as described before (Smetana et al., 2019). Root sections were stained in 1× PBS solution containing 0.1% calcofluor for cell wall staining.

Microscopy and image processing

Intact LR/LRP observation and tracing in a time-course manner was performed under the fluorescence stereo microscope (Leica M165 FC). GUS-stained root samples were first fixed into 4% paraformaldehyde solution overnight, followed by an incubation in ClearSee solution (Kurihara et al., 2015) for at least 2 days before LRs/LRPs observation and quantification under a standard wild filed microscope (Leica 2500). Confocol microscopy (Leica SP8) of the lateral view of LRs/LRPs involves fixing root samples in a 4% paraformaldehyde solution overnight, followed by incubation in ClearSee for at least 2 days, and 1-day cell wall staining with 0.1% calcofluor dissolved in ClearSee. This method was also used for lateral view observation of reporter expressions in LRP. The cross-sections of WT and cambium defective mutants were stained sequentially in a 0.05% (w/v) ruthenium red solution (Fluka Biochemika) and a 0.05% (w/v) toluidine blue solution (Smetana et al., 2019) in deionized water before observation. The figures were organized in PowerPoint. Images for LR tracing sometimes were adjusted in brightness and contrast for better visualization. Images used for comparison were always captured and displayed with the same settings.

Quantifications and statistics

Root length quantification in 7-day-old roots were performed by first scanning the plates where the seedlings were grown then measuring root length in scanned images with Fiji-ImageJ. Emerged LR numbers of WT roots and cambium defective mutant roots after a 3-day auxin or mock treatment were quantified by first subjecting the seedlings to a 70°C oven for 2 h to prevent further growth, then placing roots on a glass slide with a ruler underneath and counting root numbers every 0.5 cm. The numbers of emerged LRs in ectopic overexpression lines of cambium regulators were counted under the stereo microscope, after an 8-day germination on mock or induction growth medium. Fluorescence intensity of different cambium reporters within XPP cell lineage was quantified using Fiji-ImageJ.

Plots were created using the boxplot function and the ggplot2 package in RStudio (https://www.rstudio.com/) with R version 4.3.3 (https://www.r-project.org/). The boxplots show the first quartile (bottom of the boxes), median (middle line), and third quartile (top of the boxes). Individual

samples are represented by dots. All experiments were conducted at least twice. Statistical analyses were performed with SPSS Statistics version 29 and RStudio (https://www.rstudio.com/) using R version 4.3.3 (https://www.r-project.org/). For comparing two groups, the Welch's *t*-test was applied following the performance of a Shapiro test. For multiple group comparisons, one-way ANOVA was conducted in SPSS Statistics version 29. Levene's test assessed the homogeneity of variances. Significant differences between datasets were determined using either the Tukey post hoc test (for equal homogeneous variance) or Tamhane's post-test (for unequal variance) at a significance level of alpha = 0.05.

DATA AND CODE AVAILABILITY

All vectors and plant material in this study are available from the corresponding authors Xin Wang and Ari Pekka Mähönen upon request.

FUNDING

This work was supported by the Academy of Finland (grant numbers 316544 and 346141 to A.P.M.); European Research Council (ERC-CoG CORKtheCAMBIA, agreement 819422 to X.W., L.Y., J.Z., and A.P.M.); and the Wallenberg Academy Fellowship from the Knut and Alice Wallenberg Foundation (to C.W.M.). X.W. was also supported by a grant from the Chinese Scholarship Council (CSC).

ACKNOWLEDGMENTS

We thank J. López Ortiz, X. Zhang, H. Iida, M. Lyu, and T. Blomster for providing feedback on the manuscript. We thank H. Mulvey for help cloning the XPP inducible promoter. Confocal imaging was supported by the Light Microscopy Unit (LMU), University of Helsinki. The authors also acknowledge the use of ChatGPT for wording improvement and take full responsibility for the content of the publication. No conflict of interest declared.

AUTHOR CONTRIBUTIONS

X.W. and A.P.M. designed the experiments, and X.W. performed all experiments with the help of L.Y. L.Y. performed statistical analysis. J.Z. and C. W.M. provided unpublished material. X.W. and A.P.M. wrote the paper with input from all authors.

SUPPLEMENTAL INFORMATION

Supplemental information is available at *Molecular Plant Online*.

Received: November 13, 2024
Revised: July 2, 2025
Accepted: September 6, 2025
Published: September 8, 2025

REFERENCES

Andersen, T.G., Naseer, S., Ursache, R., Wybouw, B., Smet, W., De Rybel, B., Vermeer, J.E.M., and Geldner, N. (2018). Diffusible repression of cytokinin signalling produces endodermal symmetry and passage cells. Nature **555**:529–533. https://doi.org/10.1038/nature25976.

Atta, R., Laurens, L., Boucheron-Dubuisson, E., Guivarc'h, A., Carnero, E., Giraudat-Pautot, V., Rech, P., and Chriqui, D. (2009). Pluripotency of Arabidopsis xylem pericycle underlies shoot regeneration from root and hypocotyl explants grown in vitro. Plant J. **57**:626–644. https://doi.org/10.1111/j.1365-313X.2008.03715.x.

Beeckman, T., Burssens, S., and Inzé, D. (2001). The peri-cell-cycle in Arabidopsis. J. Exp. Bot. **52**:403–411. https://doi.org/10.1093/jexbot/52.suppl_1.403.

Benková, E., Michniewicz, M., Sauer, M., Teichmann, T., Seifertová, D., Jürgens, G., and Friml, J. (2003). Local, efflux-dependent auxin gradients as a common module for plant organ formation. Cell **115**:591–602. https://doi.org/10.1016/s0092-8674(03)00924-3.

Bielach, A., Podlesáková, K., Marhavy, P., Duclercq, J., Cuesta, C., Müller, B., Grunewald, W., Tarkowski, P., and Benková, E. (2012). Spatiotemporal regulation of lateral root organogenesis in Arabidopsis by cytokinin. Plant Cell **24**:3967–3981. https://doi.org/10.1105/tpc.112.103044.

Blilou, I., Xu, J., Wildwater, M., Willemsen, V., Paponov, I., Friml, J., Heidstra, R., Aida, M., Palme, K., and Scheres, B. (2005). The PIN auxin efflux facilitator network controls growth and patterning in *Arabidopsis* roots. Nature **433**:39–44. https://doi.org/10.1038/nature03184.

Chang, L., Ramireddy, E., and Schmülling, T. (2013). Lateral root formation and growth of Arabidopsis is redundantly regulated by cytokinin metabolism and signalling genes. J. Exp. Bot. **64**:5021–5032. https://doi.org/10.1093/jxb/ert291.

Chang, L., Ramireddy, E., and Schmülling, T. (2015). Cytokinin as a positional cue regulating lateral root spacing in Arabidopsis. J. Exp. Bot. **66**:4759–4768. https://doi.org/10.1093/jxb/erv252.

Chen, L., Wang, F., Wang, X., and Liu, Y.G. (2013). Robust one-tube Omega-PCR strategy accelerates precise sequence modification of plasmids for functional genomics. Plant Cell Physiol. **54**:634–642. https://doi.org/10.1093/pcp/pct009.

Colón-Carmona, A., You, R., Haimovitch-Gal, T., and Doerner, P. (1999). Technical advance: spatio-temporal analysis of mitotic activity with a labile cyclin-GUS fusion protein. Plant J. **20**:503–508. https://doi.org/10.1046/j.1365-313x.1999.00620.x.

De Rybel, B., Vassileva, V., Parizot, B., Demeulenaere, M., Grunewald, W., Audenaert, D., Van Campenhout, J., Overvoorde, P., Jansen, L., Vanneste, S., et al. (2010). A novel aux/IAA28 signaling cascade activates GATA23-dependent specification of lateral root founder cell identity. Curr. Biol. **20**:1697–1706. https://doi.org/10.1016/j.cub.2010.09.007.

De Smet, I., Tetsumura, T., De Rybel, B., Frei dit Frey, N., Laplaze, L., Casimiro, I., Swarup, R., Naudts, M., Vanneste, S., Audenaert, D., et al. (2007). Auxin-dependent regulation of lateral root positioning in the basal meristem of *Arabidopsis*. Development **134**:681–690. https://doi.org/10.1242/dev.02753.

Du, Y., and Scheres, B. (2017). PLETHORA transcription factors orchestrate de novo organ patterning during *Arabidopsis* lateral root outgrowth. Proc. Natl. Acad. Sci. USA **114**:11709–11714. https://doi.org/10.1073/pnas.1714410114.

Du, Y., and Scheres, B. (2018). Lateral root formation and the multiple roles of auxin. J. Exp. Bot. **69**:155–167. https://doi.org/10.1093/jxb/erx223.

Duan, L., Dietrich, D., Ng, C.H., Chan, P.M.Y., Bhalerao, R., Bennett, M.J., and Dinneny, J.R. (2013). Endodermal ABA signaling promotes lateral root quiescence during salt stress in *Arabidopsis* seedlings. Plant Cell **25**:324–341. https://doi.org/10.1105/tpc.112.107227.

Dubrovsky, J.G., Gambetta, G.A., Hernández-Barrera, A., Shishkova, S., and González, I. (2006). Lateral root initiation in *Arabidopsis*: developmental window, spatial patterning, density and predictability. Ann. Bot. **97**:903–915. https://doi.org/10.1093/aob/mcj604.

Dubrovsky, J.G., Sauer, M., Napsucialy-Mendivil, S., Ivanchenko, M. G., Friml, J., Shishkova, S., Celenza, J., and Benková, E. (2008). Auxin acts as a local morphogenetic trigger to specify lateral root founder cells. Proc. Natl. Acad. Sci. USA **105**:8790–8794.

Dubrovsky, J.G., Napsucialy-Mendivil, S., Duclercq, J., Cheng, Y., Shishkova, S., Ivanchenko, M.G., Friml, J., Murphy, A.S., and Benková, E. (2011). Auxin minimum defines a developmental window for lateral root initiation. New Phytol. **191**:970–983. https://doi.org/10.1111/j.1469-8137.2011.03757.x.

Eswaran, G., Zhang, X., Rutten, J.P., Han, J., Iida, H., López Ortiz, J., Mäkilä, R., Wybouw, B., Planterose Jiménez, B., Vainio, L., et al.

(2024). Identification of cambium stem cell factors and their positioning mechanism. Science **386**:646–653.

Fisher, K., and Turner, S. (2007). PXY, a receptor-like kinase essential for maintaining polarity during plant vascular-tissue development. Curr. Biol. **17**:1061–1066. https://doi.org/10.1016/j.cub.2007.05.049.

Goh, T., Joi, S., Mimura, T., and Fukaki, H. (2012). The establishment of asymmetry in Arabidopsis lateral root founder cells is regulated by LBD16/ASL18 and related LBD/ASL proteins. Development **139**:883–893. https://doi.org/10.1242/dev.071928.

González-Grandío, E., Pajoro, A., Franco-Zorrilla, J.M., Tarancón, C., Immink, R.G.H., and Cubas, P. (2017). Abscisic acid signaling is controlled by a BRANCHED1/HD-ZIP I cascade in *Arabidopsis* axillary buds. Proc. Natl. Acad. Sci. USA **114**:E245–E254. https://doi.org/10.1073/pnas.1613199114.

Grutzner, R., Martin, P., Horn, C., Mortensen, S., Cram, E.J., Lee-Parsons, C.W.T., Stuttmann, J., and Marillonnet, S. (2021). High-efficiency genome editing in plants mediated by a Cas9 gene containing multiple introns. Plant Commun **2**:100135. https://doi.org/10.1016/j.xplc.2020.100135.

Himanen, K., Vuylsteke, M., Vanneste, S., Vercruysse, S., Boucheron, E., Alard, P., Chriqui, D., Van Montagu, M., Inzé, D., and Beeckman, T. (2004). Transcript profiling of early lateral root initiation. Proc. Natl. Acad. Sci. USA **101**:5146–5151. https://doi.org/10.1073/pnas.0308702101.

Hirakawa, Y., Kondo, Y., and Fukuda, H. (2010). TDIF peptide signaling regulates vascular stem cell proliferation via the WOX4 homeobox gene in *Arabidopsis*. Plant Cell **22**:2618–2629. https://doi.org/10.1105/tpc.110.076083.

Hirakawa, Y., Shinohara, H., Kondo, Y., Inoue, A., Nakanomyo, I., Ogawa, M., Sawa, S., Ohashi-Ito, K., Matsubayashi, Y., and Fukuda, H. (2008). Non-cell-autonomous control of vascular stem cell fate by a CLE peptide/receptor system. Proc. Natl. Acad. Sci. USA **105**:15208–15213. https://doi.org/10.1073/pnas.0808444105.

Hunter, K., Kimura, S., Rokka, A., Tran, H.C., Toyota, M., Kukkonen, J. P., and Wrzaczek, M. (2019). CRK2 enhances salt tolerance by regulating callose deposition in connection with PLDalpha1. Plant Physiol. **180**:2004–2021. https://doi.org/10.1104/pp.19.00560.

Ingouff, M., Selles, B., Michaud, C., Vu, T.M., Berger, F., Schorn, A.J., Autran, D., Van Durme, M., Nowack, M.K., Martienssen, R.A., and Grimanelli, D. (2017). Live-cell analysis of DNA methylation during sexual reproduction in *Arabidopsis* reveals context and sex-specific dynamics controlled by noncanonical RdDM. Genes Dev. **31**:72–83. https://doi.org/10.1101/gad.289397.116.

Ito, Y., Nakanomyo, I., Motose, H., Iwamoto, K., Sawa, S., Dohmae, N., and Fukuda, H. (2006). Dodeca-CLE peptides as suppressors of plant stem cell differentiation. Science **313**:842–845. https://doi.org/10.1126/science.1128436.

Jing, H., and Strader, L.C. (2019). Interplay of auxin and cytokinin in lateral root development. Int. J. Mol. Sci. **20**:486. https://doi.org/10.3390/ijms20030486.

Kareem, A., Radhakrishnan, D., Wang, X., Bagavathiappan, S., Trivedi, Z.B., Sugimoto, K., Xu, J., Mähönen, A.P., and Prasad, K. (2016). Protocol: a method to study the direct reprogramming of lateral root primordia to fertile shoots. Plant Methods **12**:27. https://doi.org/10.1186/s13007-016-0127-5.

Karimi, M., Inzé, D., and Depicker, A. (2002). GATEWAY vectors for Agrobacterium-mediated plant transformation. Trends Plant Sci. **7**:193–195. https://doi.org/10.1016/s1360-1385(02)02251-3.

Kim, S.H., Bahk, S., Nguyen, N.T., Pham, M.L.A., Kadam, U.S., Hong, J.C., and Chung, W.S. (2022). Phosphorylation of the auxin signaling transcriptional repressor IAA15 by MPKs is required for the suppression of root development under drought stress in Arabidopsis. Nucleic Acids Res. **50**:10544–10561. https://doi.org/10.1093/nar/gkac798.

Köllmer, I., Novák, O., Schmülling, T., Schmülling, T., and Werner, T. (2014). Overexpression of the cytosolic cytokinin oxidase/dehydrogenase (CKX7) from *Arabidopsis* causes specific changes in root growth and xylem differentiation. Plant J. **78**:359–371. https://doi.org/10.1111/tpj.12477.

Kretzschmar, K., and Watt, F.M. (2012). Lineage tracing. Cell **148**:33–45. https://doi.org/10.1016/j.cell.2012.01.002.

Kurihara, D., Mizuta, Y., Sato, Y., and Higashiyama, T. (2015). ClearSee: a rapid optical clearing reagent for whole-plant fluorescence imaging. Development **142**:4168–4179. https://doi.org/10.1242/dev.127613.

Labun, K., Montague, T.G., Krause, M., Torres Cleuren, Y.N., Tjeldnes, H., and Valen, E. (2019). CHOPCHOP v3: expanding the CRISPR web toolbox beyond genome editing. Nucleic Acids Res. **47**:W171–W174. https://doi.org/10.1093/nar/gkz365.

Laplaze, L., Benkova, E., Casimiro, I., Maes, L., Vanneste, S., Swarup, R., Weijers, D., Calvo, V., Parizot, B., Herrera-Rodriguez, M.B., et al. (2007). Cytokinins act directly on lateral root founder cells to inhibit root initiation. Plant Cell **19**:3889–3900. https://doi.org/10.1105/tpc.107.055863.

Laskowski, M.J., Williams, M.E., Nusbaum, H.C., and Sussex, I.M. (1995). Formation of lateral root meristems is a two-stage process. Development **121**:3303–3310.

Li, X., Mo, X., Shou, H., and Wu, P. (2006). Cytokinin-mediated cell cycling arrest of pericycle founder cells in lateral root initiation of *Arabidopsis*. Plant Cell Physiol. **47**:1112–1123. https://doi.org/10.1093/pcp/pcj082.

Mähönen, A.P., Ten Tusscher, K., Siligato, R., Smetana, O., Díaz-Triviño, S., Salojärvi, J., Wachsman, G., Prasad, K., Heidstra, R., and Scheres, B. (2014). PLETHORA gradient formation mechanism separates auxin responses. Nature **515**:125–129. https://doi.org/10.1038/nature13663.

Mäkilä, R., Wybouw, B., Smetana, O., Vainio, L., Solé-Gil, A., Lyu, M., Ye, L., Wang, X., Siligato, R., Jenness, M.K., et al. (2023). Gibberellins promote polar auxin transport to regulate stem cell fate decisions in cambium. Nat. Plants **9**:631–644. https://doi.org/10.1038/s41477-023-01360-w.

Malamy, J.E., and Benfey, P.N. (1997). Organization and cell differentiation in lateral roots of *Arabidopsis thaliana*. Development **124**:33–44. https://doi.org/10.1242/dev.124.1.33.

Marhavý, P., Bielach, A., Abas, L., Abuzeineh, A., Duclercq, J., Tanaka, H., Pařezová, M., Petrášek, J., Friml, J., Kleine-Vehn, J., and Benková, E. (2011). Cytokinin modulates endocytic trafficking of PIN1 auxin efflux carrier to control plant organogenesis. Dev. Cell **21**:796–804. https://doi.org/10.1016/j.devcel.2011.08.014.

Marrocco, K., Thomann, A., Parmentier, Y., Genschik, P., and Criqui, M.C. (2009). The APC/C E3 ligase remains active in most post-mitotic Arabidopsis cells and is required for proper vasculature development and organization. Development **136**:1475–1485. https://doi.org/10.1242/dev.035535.

Matsumoto-Kitano, M., Kusumoto, T., Tarkowski, P., Kinoshita-Tsujimura, K., Václavíková, K., Miyawaki, K., and Kakimoto, T. (2008). Cytokinins are central regulators of cambial activity. Proc. Natl. Acad. Sci. USA **105**:20027–20031. https://doi.org/10.1073/pnas.0805619105.

Moreno-Risueno, M.A., Van Norman, J.M., Moreno, A., Zhang, J., Ahnert, S.E., and Benfey, P.N. (2010). Oscillating gene expression determines competence for periodic *Arabidopsis* root branching. Science **329**:1306–1311. https://doi.org/10.1126/science.1191937.

Motte, H., Vanneste, S., and Beeckman, T. (2019). Molecular and environmental regulation of root development. Annu. Rev. Plant Biol. **70**:465–488. https://doi.org/10.1146/annurev-arplant-050718-100423.

Norris, S.R., Meyer, S.E., and Callis, J. (1993). The intron of *Arabidopsis thaliana* polyubiquitin genes is conserved in location and is a quantitative determinant of chimeric gene expression. Plant Mol. Biol. **21**:895–906.

Parizot, B., Laplaze, L., Ricaud, L., Boucheron-Dubuisson, E., Bayle, V., Bonke, M., De Smet, I., Poethig, S.R., Helariutta, Y., Haseloff, J., et al. (2008). Diarch symmetry of the vascular bundle in *Arabidopsis* root encompasses the pericycle and is reflected in distich lateral root initiation. Plant Physiol. **146**:140–148. https://doi.org/10.1104/pp.107.107870.

Randall, R.S., Miyashima, S., Blomster, T., Zhang, J., Elo, A., Karlberg, A., Immanen, J., Nieminen, K., Lee, J.Y., Kakimoto, T., et al. (2015). AINTEGUMENTA and the D-type cyclin CYCD3;1 regulate root secondary growth and respond to cytokinins. Biol. Open **4**:1229–1236. https://doi.org/10.1242/bio.013128.

Rouse, D., Mackay, P., Stirnberg, P., Estelle, M., and Leyser, O. (1998). Changes in auxin response from mutations in an AUX/IAA gene. Science **279**:1371–1373. https://doi.org/10.1126/science.279.5355.1371.

Serrano-Ron, L., Perez-Garcia, P., Sanchez-Corrionero, A., Gude, I., Cabrera, J., Ip, P.L., Birnbaum, K.D., and Moreno-Risueno, M.A. (2021). Reconstruction of lateral root formation through single-cell RNA sequencing reveals order of tissue initiation. Mol. Plant **14**:1362–1378. https://doi.org/10.1016/j.molp.2021.05.028.

Siligato, R., Wang, X., Yadav, S.R., Lehesranta, S., Ma, G., Ursache, R., Sevilem, I., Zhang, J., Gorte, M., Prasad, K., et al. (2016). MultiSite gateway-compatible cell type-specific gene-inducible system for plants. Plant Physiol. **170**:627–641. https://doi.org/10.1104/pp.15.01246.

Smetana, O., Mäkilä, R., Lyu, M., Amiryousefi, A., Sánchez Rodríguez, F., Wu, M.F., Solé-Gil, A., Leal Gavarrón, M., Siligato, R., Miyashima, S., et al. (2019). High levels of auxin signalling define the stem-cell organizer of the vascular cambium. Nature **565**:485–489. https://doi.org/10.1038/s41586-018-0837-0.

Sugimoto, K., Jiao, Y., and Meyerowitz, E.M. (2010). *Arabidopsis* regeneration from multiple tissues occurs via a root development pathway. Dev. Cell **18**:463–471. https://doi.org/10.1016/j.devcel.2010.02.004.

Van Norman, J.M., Xuan, W., Beeckman, T., and Benfey, P.N. (2013). To branch or not to branch: the role of pre-patterning in lateral root formation. Development **140**:4301–4310. https://doi.org/10.1242/dev.090548.

Vermeer, J.E.M., von Wangenheim, D., Barberon, M., Lee, Y., Stelzer, E.H.K., Maizel, A., and Geldner, N. (2014). A spatial accommodation by neighboring cells is required for organ initiation in *Arabidopsis*. Science **343**:178–183. https://doi.org/10.1126/science.1245871.

Wang, X., Mäkilä, R., and Mähönen, A.P. (2023). From procambium patterning to cambium activation and maintenance in the *Arabidopsis* root. Curr. Opin. Plant Biol. **75**:102404. https://doi.org/10.1016/j.pbi.2023.102404.

Wang, X., Ye, L., Lyu, M., Ursache, R., Löytynoja, A., and Mähönen, A.P. (2020). An inducible genome editing system for plants. Nat. Plants **6**:766–772. https://doi.org/10.1038/s41477-020-0695-2.

Wang, Z.P., Xing, H.L., Dong, L., Zhang, H.Y., Han, C.Y., Wang, X.C., and Chen, Q.J. (2015). Egg cell-specific promoter-controlled CRISPR/Cas9 efficiently generates homozygous mutants for multiple target genes in *Arabidopsis* in a single generation. Genome Biol. **16**:144. https://doi.org/10.1186/s13059-015-0715-0.

Xiao, W., Molina, D., Wunderling, A., Ripper, D., Vermeer, J.E.M., and Ragni, L. (2020). Pluripotent pericycle cells trigger different growth outputs by Integrating developmental cues into distinct regulatory modules. Curr. Biol. **30**:4384–4398.e5. https://doi.org/10.1016/j.cub.2020.08.053.

Xuan, W., De Gernier, H., and Beeckman, T. (2020). The dynamic nature and regulation of the root clock. Development **147**:dev181446. https://doi.org/10.1242/dev.181446.

Ye, L., Wang, X., Lyu, M., Siligato, R., Eswaran, G., Vainio, L., Blomster, T., Zhang, J., and Mähönen, A.P. (2021). Cytokinins initiate secondary growth in the Arabidopsis root through a set of LBD genes. Curr. Biol. **31**:3365–3373.e7. https://doi.org/10.1016/j.cub.2021.05.036.

Zhang, H., Jennings, A., Barlow, P.W., and Forde, B.G. (1999). Dual pathways for regulation of root branching by nitrate. Proc. Natl. Acad. Sci. USA **96**:6529–6534. https://doi.org/10.1073/pnas.96.11.6529.